

UNIVERSIDAD DE LAS AMÉRICAS – PUEBLA

ESCUELA DE CIENCIAS

DEPARTAMENTO DE FÍSICA Y MATEMÁTICAS



“CORE-COLLAPSE SUPERNOVAE IN DWARF IRREGULAR GALAXIES”

TESIS PROFESIONAL PRESENTADA POR:

José Antonio Robles Martínez

COMO REQUISITO PARCIAL PARA
OBTENER EL TÍTULO DE
LICENCIADO EN FÍSICA

Sta Catarina Mártir, Puebla.

Primavera 2003

UNIVERSIDAD DE LAS AMÉRICAS – PUEBLA

ESCUELA DE CIENCIAS



“CORE-COLLAPSE SUPERNOVAE IN DWARF IRREGULAR GALAXIES”

Tesis profesional presentada por,

José Antonio Robles Martínez

Como requisito parcial para obtener el Título de

Licenciado en Física

JURADO CALIFICADOR

Marco Antonio Rosales

PRESIDENTE

Elias Brinks

VOCAL Y DIRECTOR

Victor Vyslooukh

SECRETARIO

Sta Catarina Mártir, Puebla.

Mayo 2003

A Elias, por su invaluable apoyo.

Contents

1	Introduction	1
2	WHAT ARE SUPERNOVAE?	5
2.1	A brief description of a Supernova event, and Supernova types according to their origin, light curves and especially spectra	5
2.2	A summary of the two major SN mechanisms.	7
2.3	Differences between Type Ia versus Type II (and Type Ibc)	10
2.4	SNe across the electromagnetic spectrum: summary of information that can be derived about their evolution (from X-rays to radio-waves).	11
3	SUPERNOVAE AS STANDARD CANDLES	13
3.1	Measuring brightness and distances.	13
3.2	The ideal distance indicator.	15
3.3	A broad brush view of type Ia Supernovae and how they can be used as standard candles.	16
3.4	Analysis of the characteristics of core-collapse SN in order to use them as standard candles.	21
3.5	A critical appraisal of the possibilities of using SN type II-P as distance indicators: problems and prospects	28
4	DWARF IRREGULAR GALAXIES	39
4.1	A brief review of the classification of galaxies.	39
4.2	Stellar Populations	41
4.3	Where do dwarf irregular galaxies fit in the larger scheme of things?	42
5	A SUPERNOVA SEARCH IN THE LOCAL UNIVERSE	45
5.1	Supernova rates in dwarf irregular galaxies.	45
5.2	Investigation of the feasibility of a targeted search for type II supernovae of predominantly type II-P in dwarf galaxies.	49
6	CONCLUSIONS	51

7	Appendix	53
7.1	Appendix A: Hydrostatic Equilibrium	53
7.2	Appendix B: Nuclear reactions in high-mass stars (SN progenitors)	56

Chapter 1

Introduction

One of the greatest challenges in Astronomy has always been distance determination. In order to study scales, sizes and distances, many measurement methods have been developed. Some examples are parallax measurements taking as baseline the orbit of the earth around the sun. These stellar parallaxes, taken from different sides of the orbit of the earth are usable up to ~ 30 pc. Other methods are the period–luminosity relation for cepheids which with the Hubble Space Telescope has been extended to about ~ 30 Mpc, the Tully–Fisher relation and several others. Figure 1.1 shows a comparison of the main methods employed to determine distances and their usable range.

Supernovae are one of the most energetic events in the present universe. They can be observed out to cosmological distances (Leibundgut 2001; Benítez et al. 2002). The brightest Supernovae are those of type Ia (SNe Ia, details will be explained later). They stem always from a white dwarf which has gone beyond the Chandrasekhar limit (approx. $1.4 M_{\odot}$). So this specific type of SN is likely to have the same intrinsic luminosity. That is the reason why they are ideal objects to use as *distance indicators*.

Core–collapse supernovae (SNe other than SNe Ia) occur about as frequently as type Ia supernovae but, because of their origin, trace a different environment. For example, certain types of dwarf irregular galaxies are or have been active in forming massive giant and super–giant stars, the progenitors of core–collapse supernovae. Hence the idea to target this type of supernovae (or perhaps a subclass of them) to analyze if they would be good distance indicators (with approximately the same luminosity for each event). The next step is then to calculate the core–collapse supernova rate in dwarf irregular galaxies to see if it is worthwhile to search in such galaxies for them.

If core–collapse SNe could be used (like SN Ia) as distance indicators, they could be used to measure the distance to their dwarf galaxy hosts. Moreover if, as predicted by modern cosmology, dwarf galaxies were more abundant at early times in the life of the universe, it should be possible to use core–collapse supernovae to measure the distances of the host galaxies at cosmological distances.

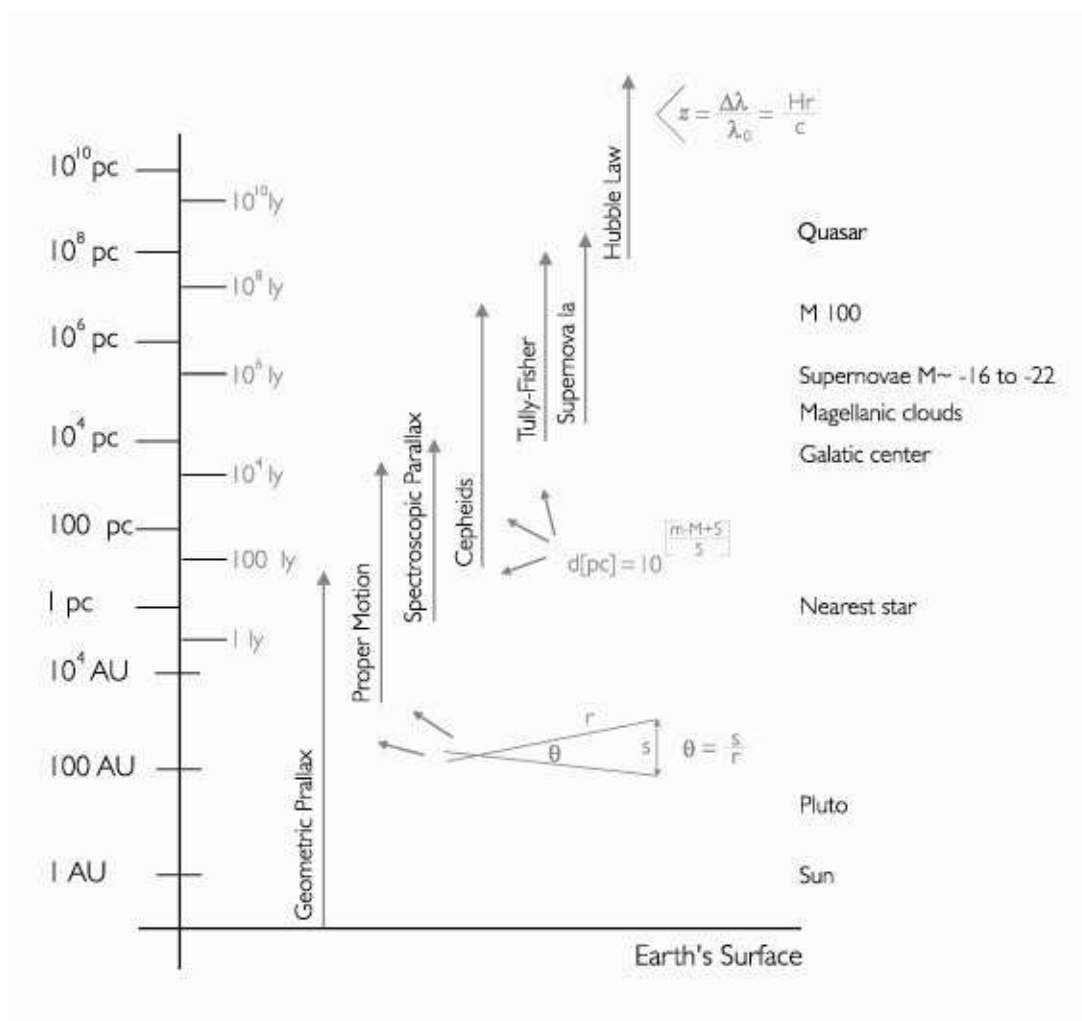


Figure 1.1: Methods and used to determine distances ranked according to their usable range ($1\text{pc} \approx 3.25$ ly).

This thesis is organized as follows: in chapter 2, we present a review of our knowledge about Supernovae and all their types and subtypes by first analyzing the two major SN explosion mechanisms and progenitor types, making a comparison between different types and subtypes based on their light curves and spectra. In chapter 3 we give some definitions of luminosities and magnitudes, followed by an overview of the uses of type Ia SNe as a distance indicator, including aspects of their homogeneity and heterogeneity as a class. We end chapter 3 with a review of the feasibility of using core–collapse supernovae as standard candles reviewing all subtypes and summarizing three independent studies discussing the advantages and disadvantages of using a specific core–collapse SN subclass. In chapter 4, after a broad brush view of the classification of galaxies and stellar populations, the star formation rate for a dwarf irregular galaxy is calculated. Lastly, in chapter 5 there is an analysis of four independent SN searches and catalogues according to SN and galaxy morphological type. Lastly, a calculation of the supernova rate in dwarf galaxies is derived and an investigation made of the feasibility of a targeted core collapse SN search in dwarf irregular galaxies, in order to evaluate their use as distance indicator.

Chapter 2

WHAT ARE SUPERNOVAE?

2.1 A brief description of a Supernova event, and Supernova types according to their origin, light curves and especially spectra

Supernovae are the explosions of certain stars in their final evolutionary stage. Supernovae come from different types of progenitor stars, from stars at least eight times more massive than our sun, and from stars (white dwarfs) with $1.4 M_{\odot}$. A supernova releases an incredible amount of energy and can be as bright as its host galaxy. It is doubtless one of the most spectacular and violent events in the universe.

There are a wide range of supernova (SN) types and subtypes depending on the characteristics of their progenitor stars. A classification is made according to the chemical elements found in their spectra. The two main types of SNe are Type I (SNe I) in which case no Hydrogen is found in their spectra, and Type II (SNe II) when a strong presence of H is found. This distinction was first made by Minkowsky in 1941. SNe I were believed to come from old low-mass stars while SNe II were ascribed to explosions of very massive stars. A problem arose when around 1985 strong presence of Helium was seen in some SNe I spectra. Furthermore, these SNe were found in populations of high-mass stars. These SNe combined properties of SN I, showing no H in their spectra and properties of SN II, those having very massive stars as progenitors. They were classified as SNe Type Ib. Then some SNe were encountered with little or no presence of He, so SNe Type Ic was consigned to these kind of SNe (SNe Ib & SNe Ic are commonly referred to as Type Ibc for simplicity).

Subtypes of SN II are assigned according to their light curve, which is the plot of the SN absolute magnitude [proportional to the logarithm of the flux] versus time [days] after the SN explosion (it can be plotted at any wavelength but optical is most commonly used). This useful tool tells us the behavior of the SN luminosity evolution, helps to decide, combined with spectral analysis, the type and subclasses of the SNe and whether or not it is feasible

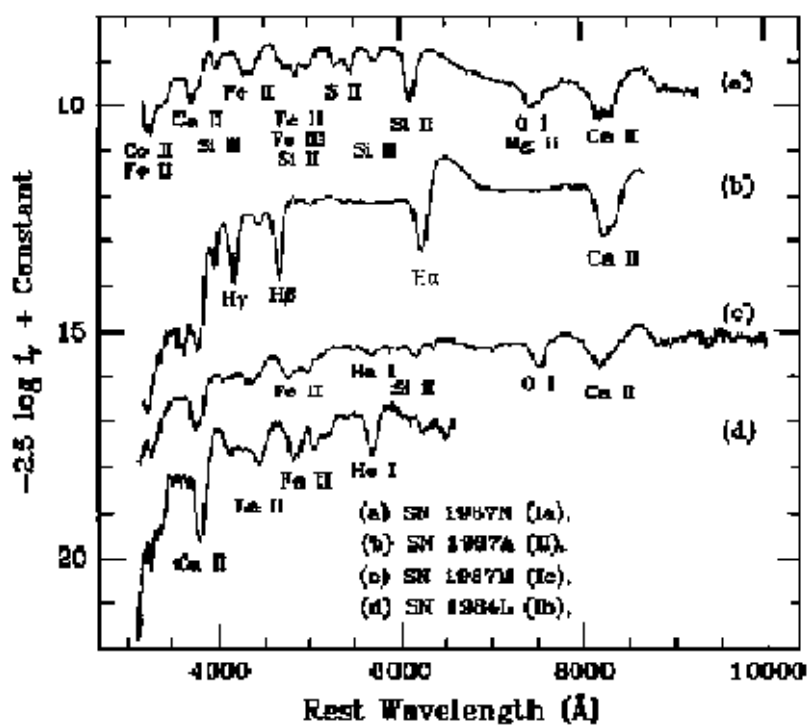


Figure 2.1: Spectra of SNe, showing distinctions between the four major types and subtypes of SNe. All spectra were taken approximately one week after peak brightness (Filippenko et al. 1997).

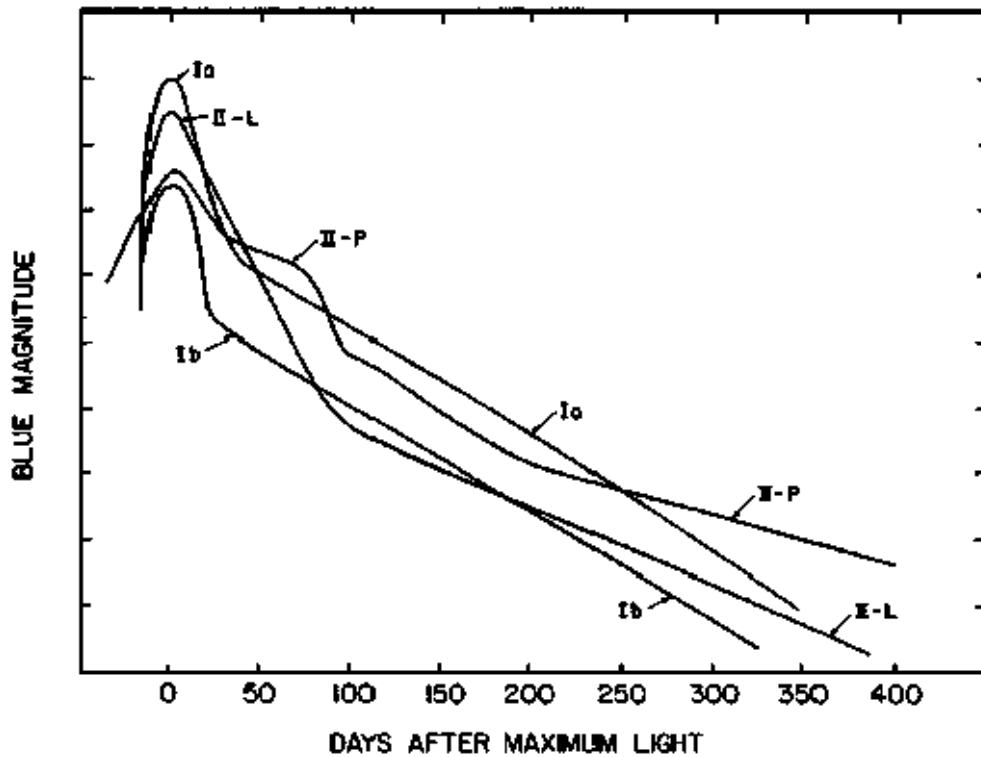


Figure 2.2: Schematic light curves for SNe of Types Ia, Ib, II-L, and II-P. The curve for SNe Ib includes SNe Ic as well, and represents an average (Wheeler et al. 1990).

to make a deeper study of that specific SN event.

If the light curve of a SN II presents linear luminosity decay with time it is considered a Linear Type II SN (SN II-L). If it presents a plateau after reaching the maximum brightness it is considered a SNe II-P. Furthermore, there exists a subtype called “Type II_n”, the “n” denoting “narrow” emission line components (Filippenko et al. 1997), most notably H_{α} . Lastly, there is a special group of SNe II called Peculiar (SNe IIpec) which are difficult to classify due to the heterogeneity of their spectra and, especially, their light curves.

2.2 A summary of the two major SN mechanisms.

Supernovae Type Ib, Ic and II: SNe II and SN Ibc are produced by the core collapse of a very massive star (more massive than about $\sim 8 M_{\odot}$) which has arrived at its final evolutionary stage. First we have to present a rough view of the evolution of a giant star. These kinds of star are so massive that, in order to maintain *hydrostatic equilibrium* (see Appendix A) between gravity and radiation pressure, they have to “burn” (in reality nuclear fusion)

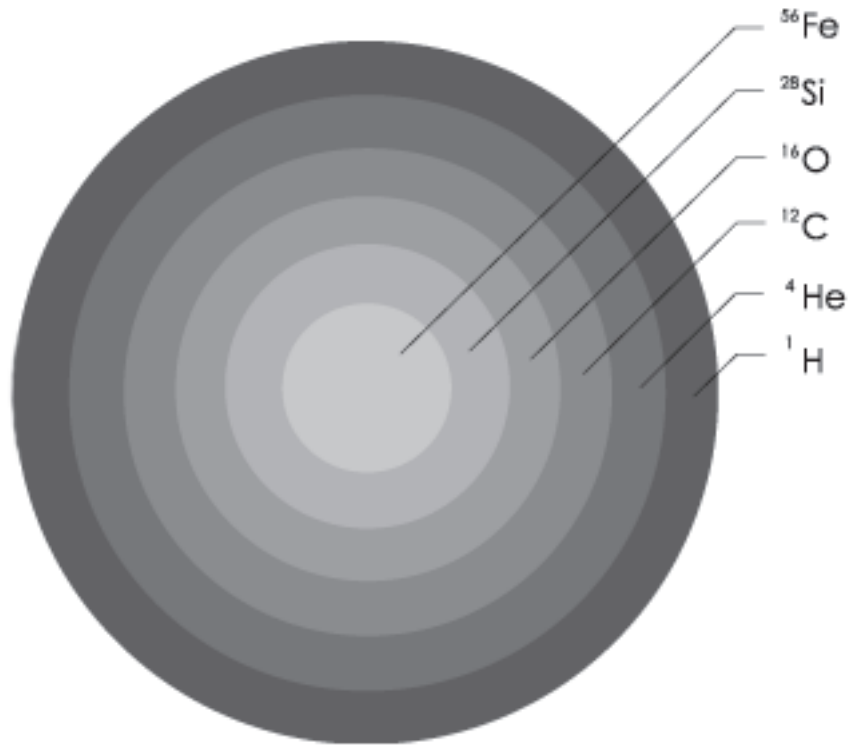


Figure 2.3: The structure of a super-massive star ($\sim 30 M_{\odot}$). At its final evolutionary stage, the star consists of layers with different composition divided by nuclear burning shells (Karttunen et al. 1993).

extremely fast the H in the nucleus, which eventually is consumed and transformed into Helium (He). When this happens the star is not able to support gravity any longer so it is compressed until the nucleus (now made of He) gets to high enough temperatures and pressures to initiate once more nuclear fusion via the triple- α process. This chain of fusion continues to produce heavier elements (the heavier the element to fuse the less energy efficient is the process) until the nucleus gets converted to Iron (see Appendix B for the stellar nuclear reactions). At this point, because Iron is the element with the highest binding energy, there is no longer fusion possible to form heavier elements. Any nuclear reaction which involves Fe will break up the Fe nucleus instead of forming a heavier one, hence not liberating energy but consuming it. From that moment, the star is no longer able to produce any significant energy to support the crushing force of gravity (Figure 2.3).

At this point, the core collapses under the tremendous pressure of the outer layers, producing an implosion shockwave, which causes degeneration of the nucleus until only

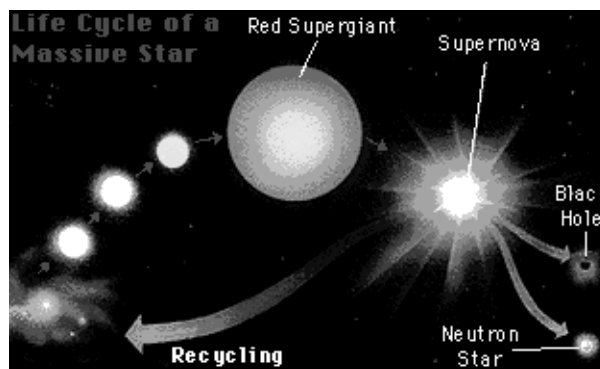


Figure 2.4: The life cycle of a super-massive star, from its formation to the final Supernova remnant: a Neutron star or Black hole (<http://www.colorado.edu>).

neutrons remain in the core¹. At that moment the nucleus becomes stable² to further collapse and suddenly the contraction stops, bouncing back and releasing so much energy that this produces an explosion shockwave which will blow the outer layer away at approximate velocities between 10^6 and 10^7ms^{-1} . This explosion is the famous SN (Figure 2.4).

Supernovae Type Ia: Supernovae of Type Ia come from a totally different process. They are unlike other SNe (Ibc and II) which are produced from a core collapse of a giant or supergiant star. This kind of SNe are produced when in a binary system composed of a white dwarf³ and a star, the companion star evolves away from the main sequence to become a giant or supergiant. Its size increases allowing the external layers of the star to get sufficiently close to the white dwarf to transfer mass from the giant (or supergiant) star to the white dwarf. In this process the transferred mass falls on to an accretion disk, and eventually will cause the white dwarf to exceed the Chandrasekhar limit (which is about $1.4 M_{\odot}$). The degenerated material of the star acquires enough mass to initiate nuclear reactions under the huge gravitational force that enhances nuclear fusion, not only in the core but throughout the white dwarf. At that moment the energy production is so violent that it suddenly overcomes gravity and explodes as the most powerful SN of all types known, reaching at the maximum of the light curve the highest peak luminosity of any SN type. This implies some exceptional qualities, such as all SNe Ia having approximately the same brightness due to their almost identical origin: the explosion of a $1.4 M_{\odot}$ white dwarf.

¹This phenomenon happens when the force of gravity compresses the electrons so much that they are forced into the atomic nucleus, causing them to combine with the protons producing total charge nullification and converting p^+ to n.

²If the progenitor star was even more massive, it is believed that not even the neutron pressure can stop the contraction. This will inevitably lead to a black hole.

³A white dwarf is the remnant of an evolved medium-size star, which lost its outer layers as a Planetary Nebula.

2.3 Differences between Type Ia versus Type II (and Type Ibc)

We can say that SNe Ibc and SNe II are the “victory” of gravity over the nuclear energy production in the core. When the star ran out of fusionable elements this caused the implosion of the core. Here the outer layers bounce back in an explosion shockwave leaving a neutron star (or in some occasions a black hole) as a remnant. On the other hand we can see the SNe Ia as the “victory” of nuclear energy over gravity when the degenerated material of the white dwarf got from an external source enough material to exceed the Chandrasekhar limit. This results in the fusion of the entire star, all at once, leading to an explosion in which the star gets totally disrupted. We mention here that the companion star at the moment of the explosion was orbiting the white dwarf, so when this one explodes, the companion can get expelled, traveling at high-speed.

These obvious differences imply totally different characteristics and behavior of the spectra and light curves. Some of the most significant are: because SNe Ia come from a degenerated star which exceeds the Chandrasekhar limit ($1.4 M_{\odot}$) it is reasonable to assume that it explodes with approximately the same amount of energy. So it will be reasonable to expect the same brightness at the light curve maximum making SNe Ia ideal probes to be used as distance indicators⁴ (standard candles). On the other hand, we have SNe Ibc and SNe II. These kind of SNe, are due to massive progenitors with masses between $\sim 8 M_{\odot}$ to even $100 M_{\odot}$ (this mass range allows them to explode as a SN). They have clearly different sizes, masses, composition and circumstellar media⁵ (CSM). The combination of all these parameters gives rise to heterogeneous SN behavior of the light curves and spectra. Despite this fact, SNe other than SNe Ia have begun to make several astronomers curious enough to try to explore the feasibility of using the different SN types and subtypes as standard candles, to complement the use of SN Ia as a distance indicator. Table 2.1 shows a SNe taxonomy flow chart according to the elements shown in each SN spectrum and the behavior of their light curves.

⁴To use SNe Ia as Standard Candles we have to consider and normalize for brightness attenuation such as interstellar and intergalactic dust.

⁵Important differences in the CSM density and elements can actually make such significant changes to the light curve and spectra as to confuse astronomers about the type or subtype of the SN.

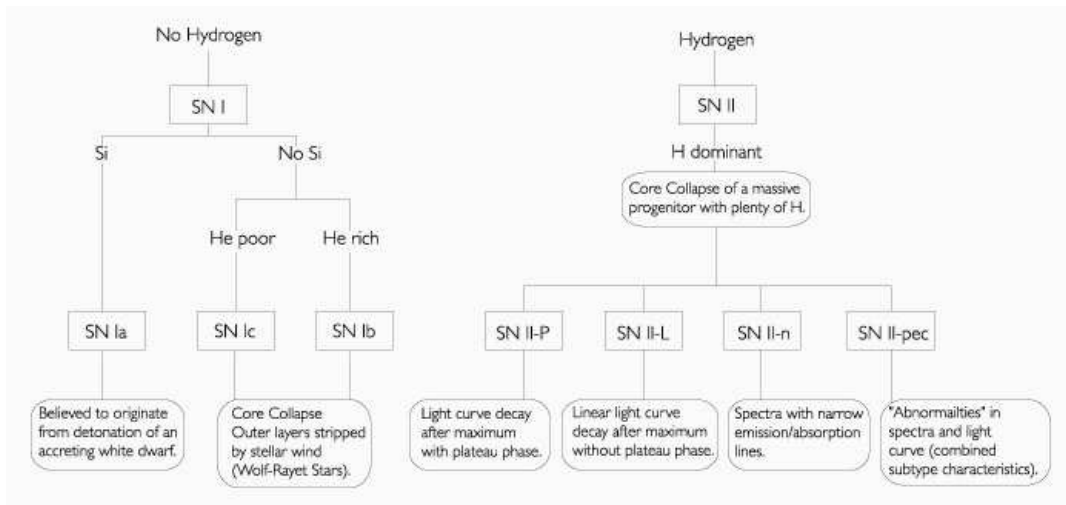


Table 2.1: Supernova taxonomy flow chart: The SN types and subtypes with the explanations of their progenitor mechanism (Based on Montes et al. 2001).

2.4 SNe across the electromagnetic spectrum: summary of information that can be derived about their evolution (from X-rays to radio-waves).

Almost all information derived about SN explosions comes from the detection of their electromagnetic radiation⁶. Commonly a SN reaches its maximum luminosity in the optical wavelength range. But due to the complex interactions involved in such an event, a SN emits electromagnetic radiation at all wavelengths. Moreover, it reaches different maximum intensities for every wavelength range at different epochs. Most phenomena are intrinsically related to the evolution of the expanding SN ejecta and their interaction with the CSM, generating shells at different densities and temperatures that radiate over a wide range of wavelengths.

Here we present a review of how it is believed that SN II emission at different wavelengths is produced:

- As reported by Pooley and Lewin (2002): soft X-rays ($\leq 10\text{keV}$) are thought to be thermal radiation from the interaction between the front of expanding SN ejecta and the CSM of the progenitor star. This collision produces a traveling “reverse” shock ($\sim 10^3 \text{ kms}^{-1}$) which collides with the ejecta, creating a dense shell with approximate temperatures of about 10^7 K which is where most of the observable X-ray emission arises.

⁶The other source of information is their neutrino flux

- The Optical, *UV*, and *IR* are also thermal radiation. Emitted from the outwards traveling SN shock which is “cooling from the breakout temperature ($\sim 10^5$ K) down to the recombination temperature of hydrogen (~ 5000 K) (Eastman, Schmidt and Kirshner 1996)”. During this period, the optical emission can be approximated as a blackbody at temperature T , fitting well the *UV*, optical and *IR* wavelengths.
- In 1982, Chevalier proposed that the outgoing shock from the SN explosion generates the relativistic electrons and enhanced magnetic field necessary for synchrotron radio emission. The ionized CSM initially absorbs most of the emission. As the shock passes rapidly outward, less ionized material is left between the shock and the observer, absorption decreases rapidly and the observed radio flux density rises (Pooley et al. 2002). Due to the absorption by the CSM and later of subsequent re-emission (first at shorter wavelengths and later at longer wavelengths Weiler et al. 1986) the radio flux arrives to the observer with a time delay which allows more time to prepare for follow up.

A huge explosion, like a SN, in addition to offering the possibility to use it to derive distances to the host galaxies in which they occur, also offers the possibility to study the many stages of the interaction between the outwards moving shock front with the CSM and pre-ejected material. The high internal temperature, the dense expanding shell, the reverse shockwave and their mutual interaction produce a great diversity of physical processes under conditions which are difficult or impossible to produce in the laboratory. Information about these processes arrives at us as electromagnetic radiation that can be observed and analyzed. So it is fitting to make the best effort in getting multiwavelength spectra and light curves which will result in a better, more comprehensive understanding of a SN event and its applications. However, for this thesis we will concentrate on one particular concept only, the potential of type II SN to be used as distance indicators.

Chapter 3

SUPERNOVAE AS STANDARD CANDLES

3.1 Measuring brightness and distances.

As mentioned in the first chapter, to be able to study distance scales, many measurement methods have been developed. A luminosity method for measuring cosmological distances consists of objects with the same *intrinsic luminosity*; this standard luminosity makes them a standard candle. We shall mention some basic concepts of electromagnetic radiation in order to derive information of its characteristics such as:

- The Intensity (I) of radiation: this is the energy passing per second through a surface element into a solid angle in a direction θ , $[I] = [Wm^{-2}Hz^{-1}sterad^{-1}]$.
- The energy flux (flux): this is the power [in Watts] going through some surface, and the flux density (generally denoted F) gives the power of radiation per unit area and per unit of frequency $[F] = [Wm^{-2}Hz^{-1}]$, note that $F \propto r^{-2}$.
- The total flux: this is the flux passing through a closed surface surrounding the source, this total flux is called the Luminosity (L), $[L] = [WHz^{-1}]$ and we can see that L is independent of distance, because the flux density falls off proportional to r^{-2} but the surrounding surface grows proportional to r^2 . Hence, the luminosity is an intrinsic property of a source.

$$F_{Tot} \equiv L = 4\pi r^2 F \tag{3.1}$$

Once we have an object with a known intrinsic luminosity (which is a challenge), the distance can be easily derived by:

$$r = \sqrt{\frac{L}{4\pi F}} \quad (3.2)$$

In Astronomy, it is more common to use absolute (M) and apparent (m) magnitudes:

- The apparent magnitude m , is defined as the received brightness from the observed object and is given by the equation:

$$m = -2.5 \log \frac{F_r}{F_0} \quad (3.3)$$

where F_r is the observed flux density and F_0 is a reference flux density corresponding to an object with apparent magnitude $m = 0$. Note that the apparent magnitude, as it deals with flux densities, depends on the distance.

- The absolute magnitude M , give us information about the real intrinsic brightness of the object. It is the apparent magnitude of an object that would have been placed at a distance of 10 parsecs from the observer.
- The relation between the apparent magnitude m , absolute magnitude M and the distance r , is the distance modulus $m - M$:

$$m - M = 5 \log \frac{r}{10pc} + A(r) \quad (3.4)$$

where r is the distance to the object in parsecs (pc) and $A(r)$ is the interstellar extinction. Usually expressed as:

$$m - M = 5 \log r - 5 + A(r) \quad (3.5)$$

$$\Rightarrow r = 10^{0.2[m-M+5-A(r)]} \quad (3.6)$$

- The absolute bolometric magnitude M_{bol} , is expressed in terms of Luminosity (total flux F):

$$M_{bol} - M_{bol\odot} = -2.5 \log \frac{F}{F_{\odot}} = -2.5 \log \frac{L}{L_{\odot}} \quad (3.7)$$

These concepts are used by astronomers to derive and calculate distances in different distance regimes. The use of equation (3.6) is called the photometric method of distance determination. This method is a direct determination of distance and its main difficulty is knowing the absolute magnitude M , which needs to be found by an independent technique. Although there are some ways to obtain M , here we will be only interested in the use of

Standard Candles. There are many objects used as standard candles, each one having its own distance range over which it operates. Examples are: Cepheid variables¹, main sequence stars², novae³, and for our particular interest: Supernovae.

3.2 The ideal distance indicator.

In order to be considered a standard candle the current available distance indicators comply with a number of basic requirements such as precisely known luminosities (for SNe) and periodicities of brightness variations (for Cepheids). In general the requirements that an ideal indicator should achieve are⁴:

- A high luminosity is obviously favored, to render the object useful as indicators useful out to the great distances that must be probed.
- It is very important that a distance indicator has the lowest possible intrinsic dispersion in its key properties, such as luminosity.
- An important requirement is the possibility of observing standard candles locally allowing accurate calibration before measurements at cosmological distances are intended.
- To anticipate problems, a firm theoretical basis for the distance indicator is required (actually, a theoretical understanding of many current distance indicators is still to be established).
- When the previous condition is not fulfilled, an empirical proof that the luminosity being used can be fully corrected for known systematic effects. Examples of variables that should be considered are: differences in chemical composition, CSM differences and interstellar reddening.
- An ideal distance indicator should also be universally available. SNe Ibc and type II are never found in elliptical and S0 galaxies because the stellar populations of these galaxies do not contain their progenitors (as we will see in chapter 4).

¹The Cepheids are stars which are pulsating. They show a relation between pulsation period and luminosity, so their absolute magnitudes can be obtained from their periods.

²The Luminosity of these stars is obtained from the Hertzsprung–Russell diagram (the plot of absolute magnitudes versus spectral types of stars).

³Novae are violent outbursts of material that has been transferred from a normal star to a white dwarf (in a binary system); when enough material is collected, the outer H shell is explosively ejected with a rapid luminosity increase. This is a recurring event as long as the white dwarf doesn't exceed the Chandrasekhar limit.

⁴This section is based on the list of requirements for an ideal distance indicator which can be found at: <http://nedwww.ipac.caltech.edu/level5/cepheids/cepheids20.html>

- The ideal situation would be to be able to find wherever and whenever needed the distance indicator of choice, rather than singular events, sporadically or unpredictably. SNe of all types suffer from this problem.
- The identification of an ideal distance indicator should be unambiguous. SNe suffer from the growing diversity of types and subtypes of SNe II (as opposed to SN Ia), thus further observations are needed to resolve differences allowing eventually an accurate classification.

Clearly, it is not likely that we will find in the future the distance indicator fitting all these criteria. However the better the corrections and the fewer the uncertainties the easier it is to extend the distance ranges and accuracies of each standard candle. When Cepheids were first used as standard candles the maximum distance operation was perhaps 5 Mpc; with the Hubble space telescope this has been extended up to ~ 30 Mpc. So it is reasonable to expect that growing technical possibilities and improved observational techniques will reveal other probes which can serve as reliable distance indicators.

3.3 A broad brush view of type Ia Supernovae and how they can be used as standard candles.

SNe Ia have long been proposed as good distance indicators for cosmology, because of their almost identical peak luminosity. Small differences can be normalized by corrections based on their individual light–curve shapes (Leibundgut et al. 2001). Due to their origin, the detonation of a $1.4 M_{\odot}$ white dwarf (as explained in 2.2), it is believed that SNe Ia explode with approximately the same amount of energy. So it is reasonable to expect the same brightness at the maximum of each light curve, making SNe Ia ideal to be used as standard candles.

SNe Ia have long been used as a successful distance indicator by many astronomers to derive distances over a wide range of distance scales. Examples of their uses are: calculation of the distance to their host galaxies in the local volume, deriving an approximation of the Hubble constant and cosmological studies of the expansion and geometry of the universe, among others. Recent studies with SNe Ia, suggest the possibility that the expansion of the Universe is accelerating at the current epoch (Riess et al. 1998; Perlmutter et al. 1999)

Here we present a brief review of the countless concepts, observations, and conclusions by many experts since SNe Ia were first proposed as a means to determine distances and cosmological parameters by Wilson (1939).

The light curves of SNe Ia have an overall homogeneity which yields a good standard candle with a quantifiable heterogeneity. Its high luminosity combined with high precision observations provides a reasonable normalization of its light curve. The photometric use of SNe Ia is possible because there exists a correlation between the light curve shapes, and its

luminosity. As reported by Jha, Kirshner and Garnavich (1993): almost all of the results obtained by the study of SN Ia, rely on photometric observations of SN Ia in the rest-frame optical B, V, R and I passbands⁵.

Spectral analysis is a basic tool to study SN evolution, its type, subtype and further information (such as distance). As mentioned by Filippenko et al. (1997); “The early-time spectra of SNe Ia exhibit prominent broad peaks and valleys. Extensive computer modeling of the expanding ejecta has resulted in reliable identifications for most features, after decades of uncertainty. In general, at very early times they are attributed to lines of neutral and singly ionized intermediate mass elements (O, Mg, Si, S, C), with some contribution from iron-peak elements (Fe, Co) especially at near- UV wavelengths (Branch et al. 1983, 1985, Harkness 1986, Kirshner et al. 1993, Mazzali et al. 1993). The strongest features are Si II $\lambda 6355$ Å and Ca II H&K $\lambda\lambda 3934, 3968$ Å. Convincing evidence for the presence of Helium has never been shown, although the results of Meikle et al. (1996) are intriguing and warrant further scrutiny”. Basically, all discussions and reports analyzing the advantages, disadvantages, certainties and uncertainties about the use of SN Ia as distance indicators can be reduced to SN Ia Homogeneity versus Heterogeneity:

- *Homogeneity*

It has been noticed since a long time that the optical spectra of SNe Ia are quite homogeneous. Although by most experts they are not considered to be truly a standard candle, having a considerable range in observed peak luminosity, they are nonetheless ranked as an excellent distance indicator useful even for cosmological studies (e.g. Riess et al. 1995a,b 1996, Hamuy et al. 1995, 1996a,b, and references therein).

Figure 3.1, shows an excellent example of the homogeneity of spectra of SN Ia; notice that all spectra are adjusted to rest wavelength, to compensate for the red-shift produced by the host galaxy velocity. According to Hamuy (1991), the optical light curve shapes of many SNe Ia are closely similar to each other, a remarkable fact taking into account the correlation between time (in days) and luminosity (or magnitude). After the analysis of a large amount of data, Leibundgut (1988) developed a pattern of light curves for a variety of bandpasses. Matching the B and V light curves of a SN Ia (SN 1990N), Leibundgut (1991) discovered two weeks before maximum brightness that this SN fitted very well the previous pattern assigned. The quantification of dispersion in the peak absolute magnitude of unreddened SNe Ia, was carried out by Branch & Miller (1993), Vaughan et al. (1995) and many others. In this quantification, only SNe Ia were included whose $B-V$ color at maximum brightness were in the range ± 0.25 mag.

⁵The passbands are the wavelength intervals observed through the filters used to allow only a certain wavelength band to enter the detector: B (blue) = 360–550 nm, V (visual) = 480–680 nm, R (red) = 530–950 nm and I (infrared) = 700–1200 nm.

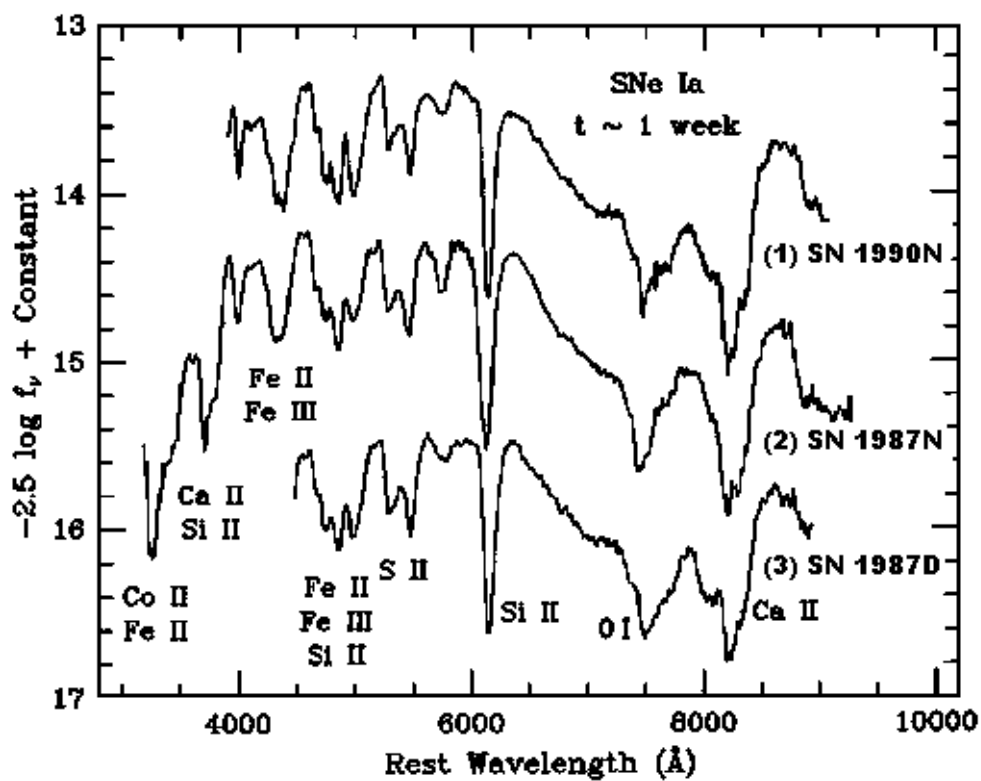


Figure 3.1: Spectra of SNe Ia about one week past maximum brightness. Where the abscisse is the wavelength [10^{-10} m = 1\AA], and ordinates are the SN magnitudes. For clarity, the spectra are plotted with an offset. The following SNe are plotted: (1) SN 1990, (2) SN 1987N, and (3) SN 1987D (Filippenko et al. 1997).

Vaughan et al. found that:

$$\langle M_B \rangle = -18.54 \pm 0.06 + 5 \log \frac{H_0}{85} \text{mag} \quad (3.8)$$

$$\langle M_V \rangle = -18.59 \pm 0.06 + 5 \log \frac{H_0}{85} \text{mag} \quad (3.9)$$

where H is the Hubble parameter and H_0 is its present value ($\sim 71 \text{ kms}^{-1} \text{Mpc}^{-1}$ Freedman et al. 2001). In the late 20's Hubble discovered that the universe is expanding with velocity proportional to the relation (Hubble law) $z = H/c \cdot r$ where $z = \lambda - \lambda_0/\lambda_0$ and r is the distance of the used object. For small velocities ($V \ll c$), the Doppler redshift $z = V/c$, and then: $V = Hr$.

Much of the measured dispersion (only 0.3 mag in both cases) is possibly due to observational errors, incorrect relative distances, and residual reddening; the intrinsic dispersion is certainly smaller.

- *Heterogeneity*

Despite several normalizations based on corrections from their light–curve shapes, careful inspection of data and analysis of spectra shows that variations among SN Ia exists. In 1987 Branch reported that the ejecta of SNe Ia do not always have the same velocity at a given phase. This fact is remarkable because different ejecta velocities will produce an intrinsic red–shift error which won't be possible to be corrected. Smallest ejection velocities are generally found among SNe Ia in elliptical galaxies (Filippenko 1989b, Branch & van den Berg 1993). These spectroscopic variations between SN Ia in spiral and elliptical galaxies, clearly show a physical diversity in the SNe Ia mechanism. This diversity is perhaps due to significant changes in CSM density and composition, or even maybe due to fundamental differences in the SNe.

Broad heterogeneity has not only been found in spectra, but also in light curves. Intrinsically bright SNe Ia rise and decline more slowly than dim ones (Phillips 1993, Hamuy et al. 1995, 1996a, Riess et al. 1995a, 1996). Such variations clearly imply differences in SNe Ia light curve shapes. Notably, the most luminous SNe Ia seem to occur in young stellar populations (Hamuy et al. 1995, Branch et al. 1996). Over the last years, there have been more reported peculiarities and differences about light curves and spectra of SNe Ia. An example of significant spectral variations among three SNe Ia is presented in figure 3.2. Note that the spectra are compared in rest wavelength. In other words, they have already been red–shift adjusted and corrected.

In conclusion, despite not being truly “standard” candles (cf. Branch & Tamman 1992, and references therein). SNe Ia are excellent and versatile tools to be used as distance indicators. Although they have a significant degree of heterogeneity, many spectroscopic and

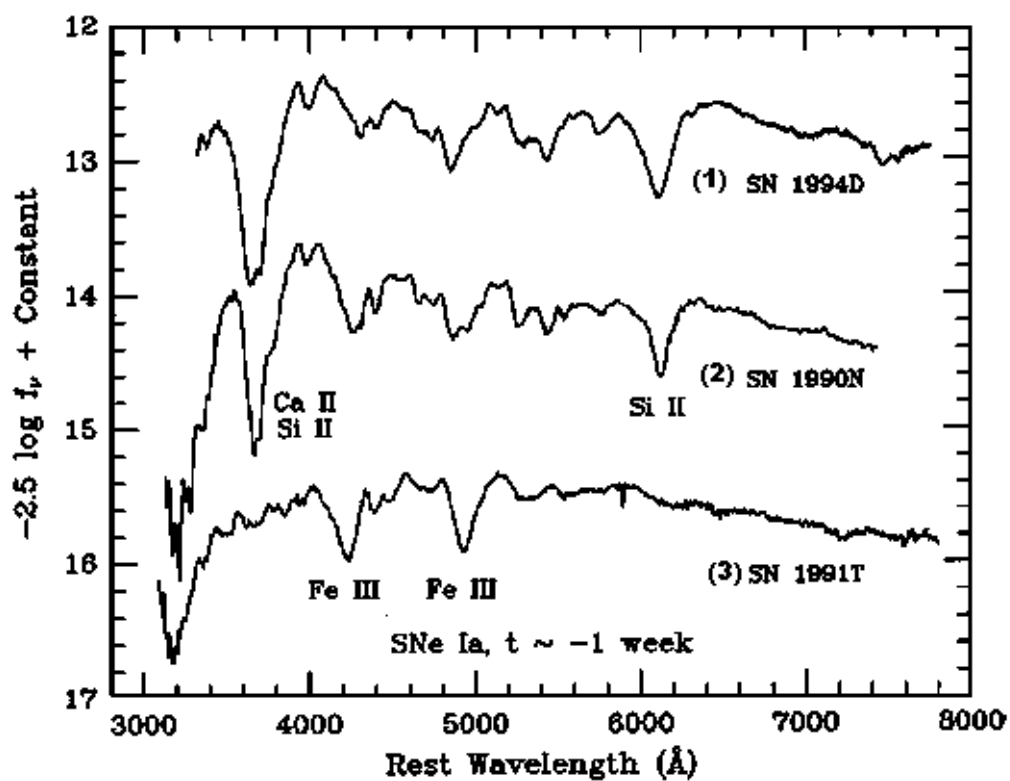


Figure 3.2: Spectra of SNe Ia about one week before maximum brightness. Spectrum heterogeneity is intrinsic. Plotted SNe are as follows: (1) SN 1994D, (2) SN 1990N, and (3) SN 1991T (Filippenko et al. 1997).

SNe Ia Average Data			
Progenitor Star type	Progenitor Mass [Solar Masses]	Bolometric Mag. ¹ <M _{bol} >	Ejecta Velocity ² (ms ⁻¹)
White Dwarf	~1.4 Solar Masses	~ -20.0 ± 0.5	~10 ⁷
Typical <SNe Ia>			
Mag. Error ³ <mag>	Mag. Error ⁴ <mag>		
~0.63 mag	~0.7 mag		

References:

¹Critical Rev of Sel Meas Tecns. (nedwwwipac.calthecc.edu)²Karttunen H. (Fundamental Astronomy)³Tammann and Leibundgut et al 1990⁴Tully et al 1998

Table 3.1:

light curve normalization techniques have been developed and proved to be successful. The versatility of SNe Ia as distance indicators is remarkable. They can be used to measure distances within the local volume, to determine the Hubble constant, to measure cosmological distances, etc. The amazing announcement that the universe is maybe increasing its expansion velocity was based on data analysis of a distant SNe Ia. Type Ia Supernovae are one of the best photometric distance indicators currently used. Table 3.1 shows an average of SN Ia main characteristics.

3.4 Analysis of the characteristics of core-collapse SN in order to use them as standard candles.

The type II and Ibc Supernovae, (as examined in Chapter 2) come from the final evolutionary stage of giant and supergiant stars. At the end point of their life these stars suffer a core collapse in which the outer layers of the star are ejected explosively at high velocities ($\sim 10^6$ and 10^7 ms⁻¹). The explosion of these massive stars is not related to a specific mass of the SN progenitor (as is the case in SN Ia ruled by the Chandrasekhar limit) but by the collapse of hydrostatic equilibrium. The star mass can vary from $\sim 7 M_{\odot}$ to $15 M_{\odot}$ for SN II and from $\sim 15 M_{\odot}$ to $100 M_{\odot}$ is thought to correspond to SN Ibc. With the combination of different sizes, masses, composition and CSM conditions, they are intrinsically infinitely heterogeneous. With this, we can readily expect variations in spectra and light curves of SN II and SN Ibc. In spite of this, studies and analysis of type II supernovae have begun, in order to find out if they can serve as standard candles.

Type Ibc SN, due to the nature of their supermassive progenitors, suffer from two intrinsic problems when considering them as potential distance indicators:

- Because the progenitor's mass range is broad ($\sim 15 M_{\odot}$ to $100 M_{\odot}$), the degree of heterogeneity of SN Ibc makes the light curve normalization less efficient and more complicated than type II SNe.
- Noting that SN Ibc progenitors are the most massive of all core-collapse supernovae, it is predicted by the Initial Mass Function (*IMF*; as will be described in chapter 5), that the formation of SN Ibc progenitors is much less favored than the formation of SN II progenitors. Their situation is directly related to the probability of finding a SN Ibc event.

Due to these facts (wide heterogeneity and low progenitor birthrate), SNe Ibc cannot be considered as a feasible distance indicator. So we will focus rather on type II SN and its subtypes.

The characterization of type II supernovae as distance indicators finds its first problem with the diversity of subtypes of SN II. Type II Supernovae are classified by the behavior in their light curve, and the lines shown in the spectra. Although it would be ideal to use all SN II, this is practically impossible. Actually, the most reasonable idea is to choose the best subtype candidate and to analyze its possibilities. Here we name the subtypes of SN II and some of their characteristics:

- *Type II-P Supernovae*

Type II plateau supernovae (SN II-P), have a plateau in their post maximum light curve. This plateau is obviously the main characteristic of this kind of SNe, which corresponds to a constant (actually a slower decay of) magnitude during 50 – 100 days. The evolution of this SN type has been reported and analyzed by several authors: Gravssberg, Imshennik, & Nadyozhin (1971), Chevalier (1976), Falk & Arnett (1977), Woosley, Weaver & Eastman (1986). The phases of the explosion can be divided in to stages: first, a shock wave originates at the center and breaks out at the star's surface in the preliminary period of cooling from the break out temperature ($\sim 10^5$ K) down to the recombination temperature of hydrogen (~ 5000 K). the second phase is an enduring era of recombination which, in red supergiant explosions, gives rise to the extended plateau observed in SNe II-P light curves. Beyond the plateau phase, the bolometric light curve tracks the instantaneous energy input rate from radioactive decay, the electron scattering optical depth is of order unity. In Figure 3.3 Filippenko (1997) notes that when the light curve drops to the late-time tail, the spectrum gradually takes a nebular appearance; the continuum fades, but H_{α} becomes very strong, and prominent emission lines of [O I], [Ca II], and Ca II also appear.

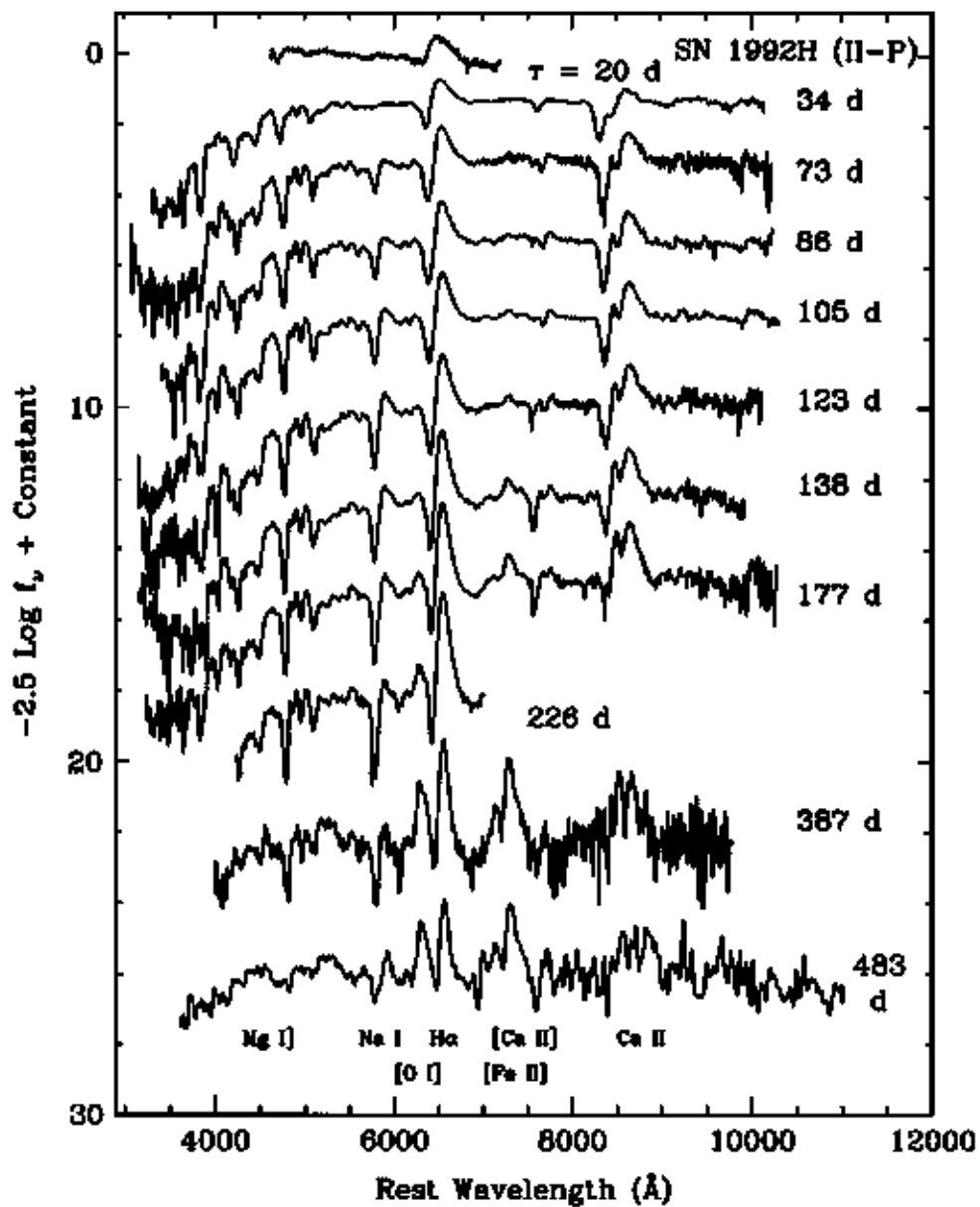


Figure 3.3: Montage of spectra of the Type II-P SN 1992H. The montage was ordered by epochs [in days]. The spectra are offset along the ordinate, for clarity (Filippenko et al. 1997).

- *Type II-L Supernovae*

Type II linear supernovae (SN II-L), are named this way, because of the linear decay of magnitude with time of their light curves. It is believed that they have relatively low mass hydrogen envelopes (a few solar masses); otherwise, they would exhibit distinct plateaus, as do SNe II-P. A different explanation of this behavior could be also a bigger extension of their Hydrogen envelope, or a CSM of larger density than SN II-P (Filippenko et al. 1997). Several authors (e.g. Wheeler & Harkness 1990) have speculated that the absence of H_α absorption differentiates spectroscopically SNe II-L from SNe II-P. Although Schlegel (1996) formally proposed that this differentiation seems to be acceptable, he admitted that a larger amount of well observed samples is needed to conclude a spectroscopic difference between SNe II-L and SNe II-P. The light curves of some SNe II-L reveal an extra source of energy: after declining exponentially for several years after outburst, the H_α flux of SN 1980K reached a steady level, showing little if any decline thereafter (Uomoto & Kirshner 1986, Leibundgut et al. 1991b). One of the major problems with SNe II-L is the small number of well observed events, thus not enough data has been available to allow experts to decide whether or not is possible to use SNe II-L as a distance indicator.

- *Type II-n Supernovae*

Type II narrow supernovae (SN II-n), are the subtype that presents narrow emission lines in their spectra, which is dominated by strong lines, most notably H_α . Chevalier (1990) made a report with the suggestion that the SN II-n intermediate-width or very narrow emission components are enhanced by the strong interaction with a high density CSM. Clearly, Type II-n supernovae show considerable heterogeneity, as detailed by observations made of some⁶ SNe II-n by Filippenko & Matheson (1993, 1994). Later, independent observations and data analysis, revealed that after years of spectra completely dominated by H_α emission of $\text{FWHM} \approx 1000 \text{ km s}^{-1}$, strong radio and X-ray emission showed up in those SN II-n with the densest CSM (Pollas et al. 1995, Garnavich et al. 1995a, Van Dyk et al. 1996b). In Figure 3.5, very strong lines of Fe II, Ca II, and O I emerged. The late time optical spectra of SN 1988Z was detected at radio wavelengths with a high luminosity, and also detected in X-rays. Recently, a considerable number of SN II-n have been observed, and they have shown a wide range of properties which renders them less favorable to use as distance indicators.

- *Type II-pec Supernovae*

Type II peculiar supernovae (SN II-pec) are basically all supernovae exhibiting enough characteristics to be considered as core-collapse supernova (with a massive

⁶SNe II-n studied by Filippenko & Matheson (1993, 1994): SN 1986J, SN 1988Z, SN 1993N.

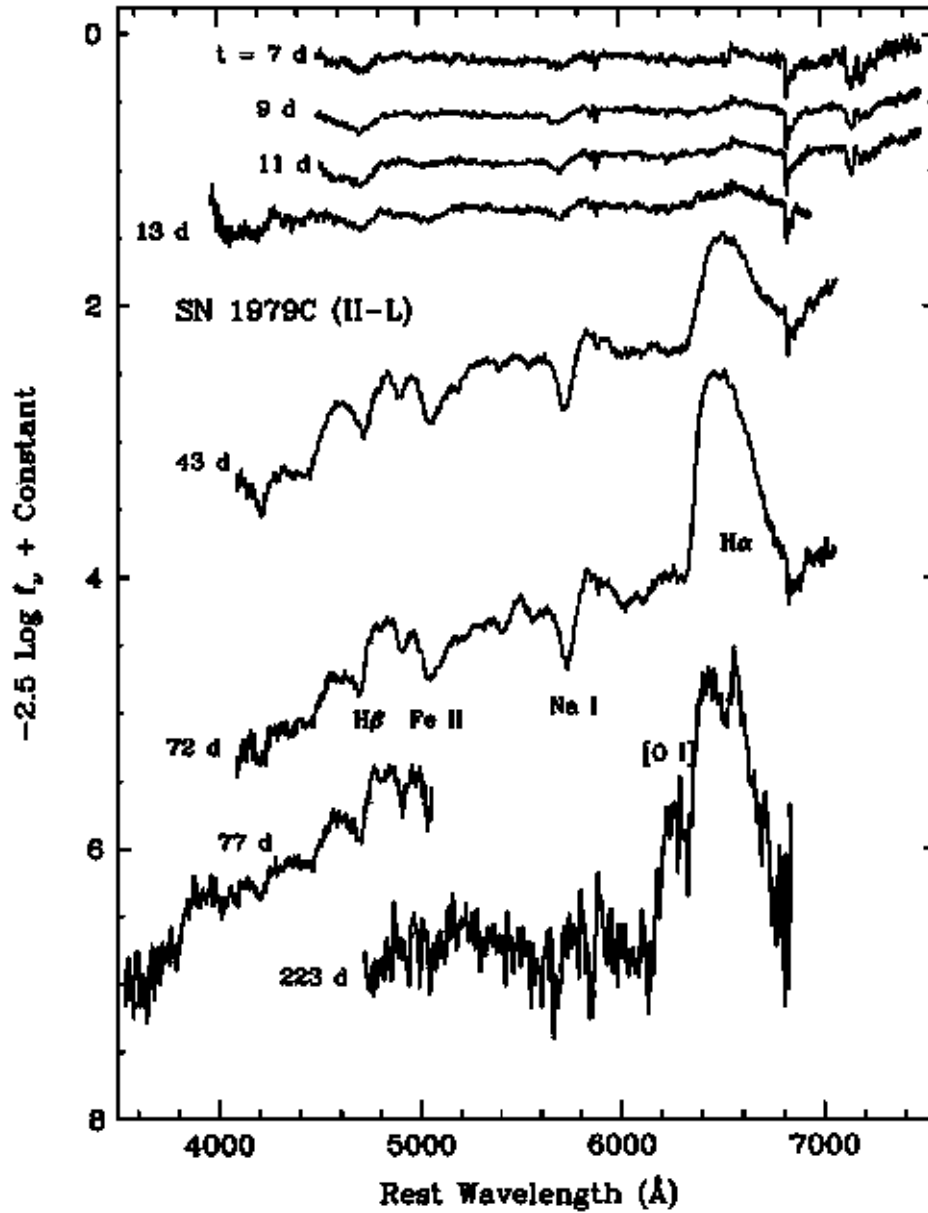


Figure 3.4: Montage of spectra of the Type II-L SN 1979C. The montage was made by epochs [in days](Branch et al. 1991).

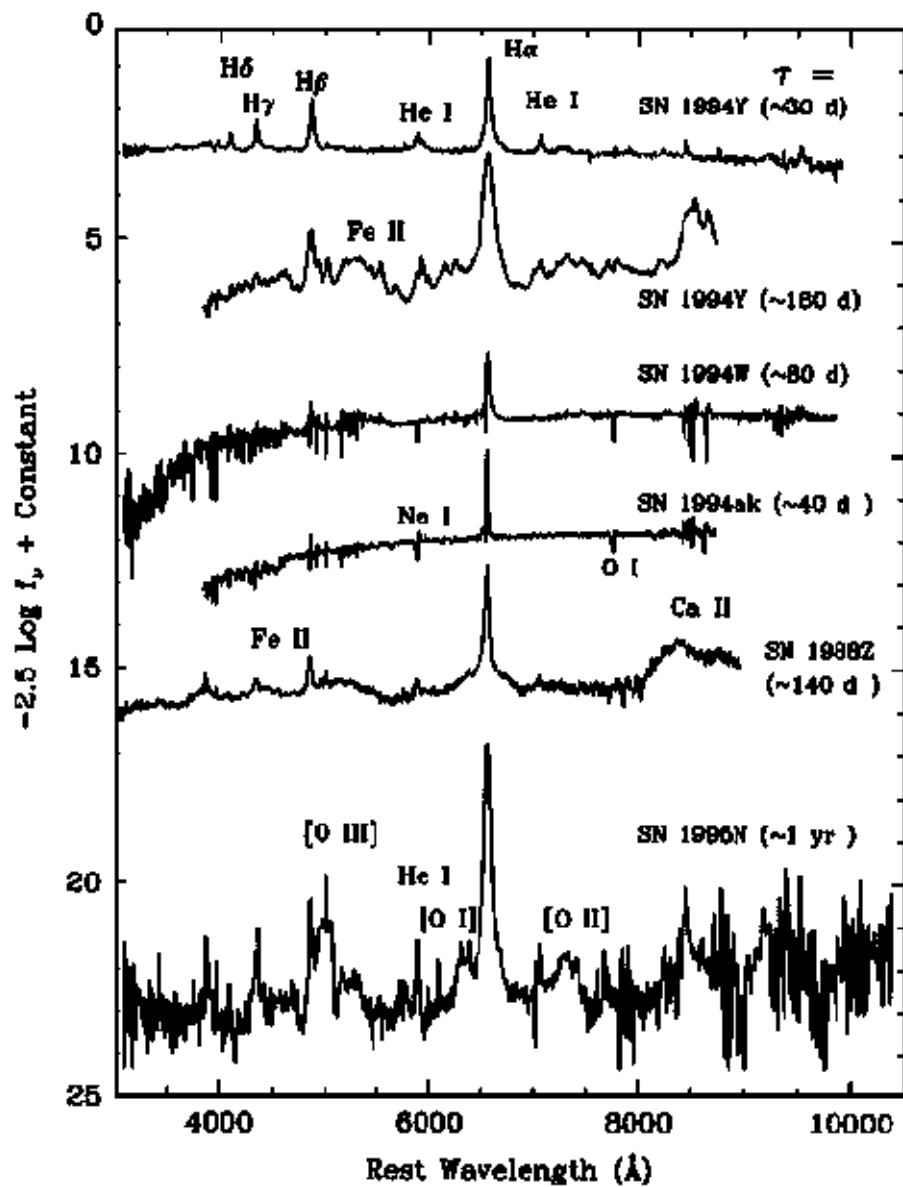


Figure 3.5: Montage of spectra of Type II-n ordered in increasing time since maximum bright [in days]. SNe II-n plotted are as follows: (1) SN 1994Y (Sept 01, 1994 & Jan 26, 1995), (2) SN 1994W (Oct 1, 1994), (3) SN 1994ak (Jan 26, 1995), (4) SN 1988Z (April 27, 1989), and SN 1995N (May 24, 1995)(Filippenko et al. 1997).

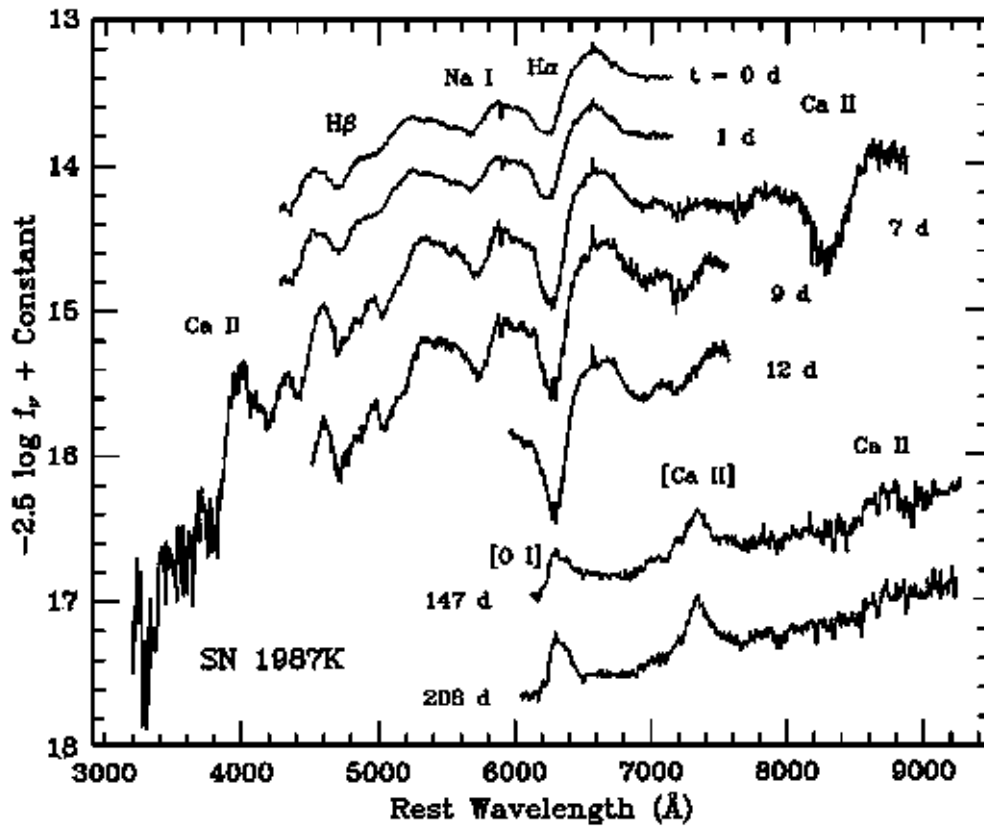


Figure 3.6: Montage of spectra of SN 1987K, showing the dramatic transformation from SN II to SN Ib. Narrow emission lines, produced by superposed HII regions, have been excised in the late time spectra. Epochs [in days] are given relative to the date of maximum brightness (adapted from Filippenko 1998).

star as progenitor), but have “abnormalities” in their spectra and light curves. Usually this kind of SN shows combined characteristics for example: narrow emission lines (from SN II–n) with low mass Hydrogen envelopes (from SN II–L). Furthermore, SNe have been found sharing characteristics between SNe II and SNe Ibc! SN 1987K (Figure 3.6) shows evidence of continuity between the progenitors and explosion mechanisms of some SNe II and SNe Ibc. Despite the fact that it is not a frequent event, sporadically SNe suffer a transformation from one type (or subtype) to another. The SN II–pec subtype of supernovae is obviously extremely heterogeneous, showing great variations in light curves and spectra. This fact prevents any possibility for normalization, and thus to use them as distance indicators.

After reviewing SN II types, it is obvious that SN II–pec as a class do not even come close to be fit as distance indicator. In the case of SN II–n, strong interaction with a high

density (possibly the densest of all SNe II) CSM, gives the net result of a wide variety of shifted wavelengths (because of absorption and reemission), and thus a high degree of heterogeneity. This carries with it the evident disqualification for our purposes.

SNe Type II–P and II–L are more homogeneous. The issue if there is continuity between SNe II–P and SNe II–L is still being debated. The main difference between them seems to be the hydrogen (H) envelopes. Whereas the envelope for SNe II–P is expected to be massive, the ones around SNe II–L are believed to be low mass H envelopes. The more massive H envelope of SNe II–P is responsible for the recombination (at $T \sim 5000$ K), giving rise to the extended plateau. The extended plateau gives useful data about explosion time, a common duration of plateau phase of ~ 80 to 150 days allowing greater photometric calibration, and a particular homogeneity condition: because the extended plateau takes place during hydrogen recombination, the major opacity contribution is controlled by H, with well known atomic properties. On the other hand, the peak absolute magnitudes of SNe II–P show a wide dispersion almost certainly due to differences in radii of the progenitor stars (Schmitz & Gaskell 1988), while most SNe II–L have a nearly uniform peak absolute magnitude (Young & Branch 1989, Gaskell 1992). However, in recent studies, it has been suggested that SNe II–P originate only in intermediate mass stars of $8\text{--}12M_{\odot}$, located in the red supergiant region (Smartt et al. 2001). This implies that SN II–P could all have similar intermediate mass progenitor stars, and the proposal that higher mass stars produce the other Type II and Ibc subtypes.

Taking into account all this information, I believe that the mass range limit imposed to the SNe II–P progenitors, set a better degree of homogeneity for this SN subtype. The reduction of dispersion allows an easier normalization of light curves and spectra. Thus, the special plateau characteristics, offers the possibility of a more accurate photometric measurement. These are the reasons why SNe II–P are chosen in the attempt of using them as distance indicators.

3.5 A critical appraisal of the possibilities of using SN type II–P as distance indicators: problems and prospects

In order to analyze the specific possibilities and the feasibility of using SN II–P as distance indicators, we are going to present a review of three independent studies where SN II–P data were extensively adjusted, analyzed, and interpreted using different methods:

i Type II Supernovae as Standardized Candles

Authors: Mario Hamuy and Philip A. Pinto (2002)

In this paper, the authors present evidence for a correlation between expansion velocities of the ejecta of Type II–P supernovae and their bolometric luminosities M_{bol} during the

plateau phase. This correlation is used to standardize the candles and decrease the scatter in the Hubble diagram from ~ 1 mag to levels of 0.4 and 0.3 mag in the V and I bands, respectively.

In this letter it is shown that the envelope expansion velocities of the II–P (Barbon, Ciatti, & Rosinno 1979) are highly correlated with their luminosities during the plateau phase, allowing to standardize the luminosities and use them to derive distances with precisions comparable to those reached by SNe Ia.

For all these SNe, precise optical photometry uncontaminated by host galaxy light was obtained. They found two relations, a relation between red–shift cz , visual magnitude V_p , and expansion velocity v_p and another identical one with near infrared magnitude I_p (This relations depend on taking V_p and v_p during the plateau phase); First, the relation for the V_p band magnitude:

$$V_p - A_V + 6.50(\pm 0.99) \log\left(\frac{v_p}{5000}\right) = 5 \log(cz) - 1.29(\pm 0.13) \quad (3.10)$$

where the A_V factor is the absorption

The second is a similar relation which holds for the I –band magnitude:

$$I_p - A_V + 5.82(\pm 0.76) \log\left(\frac{v_p}{5000}\right) = 5 \log(cz) - 1.80(\pm 0.10) \quad (3.11)$$

Bolometric light curves were derived by Hamuy (2001) for these SNe using:

- (1) BVI photometry
- (2) Empirical bolometric corrections
- (3) Reddening corrections due to our own galaxy (Schlegel, Finkbeiner, & Davis 1998).
- (4) Host galaxy extinction corrections (assuming that all SNe reach the same color at the end of the plateau).
- (5) Redshift based distances (using $H_0 = 65$).

The resulting bolometric luminosities confirmed the well–known fact that SNe II–P display a wide range (7.5 mag peak to peak) of plateau luminosities. They also noted that SNe with brighter plateaus have higher envelope expansion velocities. Figure 3.7 compares the plateau characteristic luminosity and expansion velocity of the 17 SNe II–P (all measured 50 days after explosion, corresponding approximately to the middle of the plateau). While in Figure 3.8 the redshift is compared to the visual magnitudes.

The tight luminosity–velocity correlation and the inverse square law⁷ imply that the distance to a SN II–P can be derived from measurements of the apparent magnitude and envelope velocity. Table 3.2 lists the specific data sources along with characteristic BVI magnitudes and velocities of the expanding ejecta.

⁷Inverse square law: $B_a = L_a/4\pi r_a^2$ and $B_b = L_b/4\pi r_b^2$ Then: $B_a/B_b = L_a r_b^2/L_b r_a^2$.

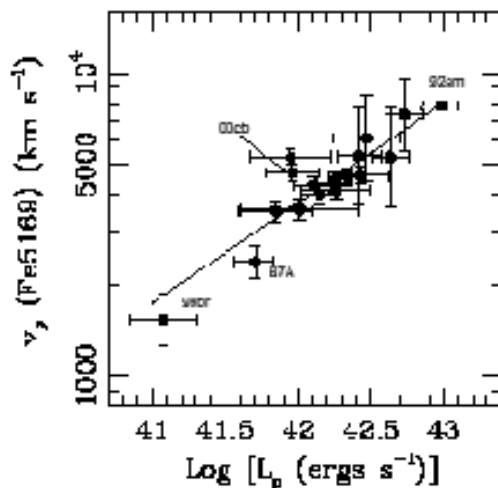


Figure 3.7: Expansion velocities from Fe II $\lambda 5169$ versus bolometric luminosity, both measured in the middle of the plateau (day 50). Ridge line is a weighted fit to the points and corresponds to $v_p \propto L_p^{0.33(\pm 0.04)}$ (Hamuy & Pinto 2002).

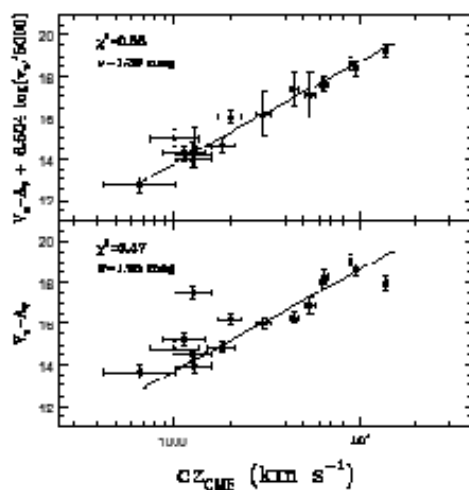


Figure 3.8: Bottom: Raw Hubble diagram from SNe II-P V magnitudes. Top: Hubble diagram from V magnitudes corrected for envelope expansion velocities (Hamuy & Pinto 2002).

Redshifts, Magnitudes, and Expansion Velocities of the 17 Type II-P SNe						
SN	cz_{CMB} ($\pm 300 \text{ km s}^{-1}$)	$A_{\text{Gal}}(V)$	$A_{\text{host}}(V)$ ($\pm 0.3 \text{ mag}$)	V_p	l_p	V_p (km s^{-1})
1986L	1293	0.99	0	14.57(05)	...	4150(300)
1987A [†]	...	0.249	0.22	3.42(05)	2.45(0.05)	2391(300)
1088A	1842	0.136	0	15.00(05)	...	4613(300)
1990E	1023	0.082	1	15.90(20)	14.56(0.2)	5324(300)
1990K	1303	0.047	0.5	14.50(20)	13.90(0.05)	6142(2000)
1991al	4484	0.168	0.15	16.62(05)	16.16(0.05)	7330(2000)
1992af	5438	0.171	0	17.06(20)	16.56(0.2)	5322(2000)
1992am	14009	0.164	0.3	18.44(05)	17.99(0.05)	7368(300)
1992ba	1165	0.193	0	15.43(05)	14.76(0.05)	3523(300)
1993A	8933	0.572	0	19.64(05)	18.89(0.05)	4290(300)
1993S	9649	0.054	0.3	18.96(05)	18.25(0.05)	4569(300)
1999br	1292	0.078	0	17.58(05)	16.71(0.05)	1545(300)
1999ca	3105	0.361	0.3	16.65(05)	15.77(0.05)	5353(2000)
1999cr	6376	0.324	0	18.33(05)	17.63(0.05)	4389(300)
1999eg	6494	0.388	0	18.65(05)	17.94(0.05)	4012(300)
1999em	669	0.13	0.18	13.98(05)	13.35(0.05)	3557(300)
2000cb	2038	0.373	0	16.56(05)	15.96(0.05)	4732(300)

SNe also analyzed by Eastman, Schmidt, and Kirshner (1996).
[†] SN also analyzed by Weiler et al. (1998).

Table 3.2:

The scatter drops from 0.95 to 0.39 *mag*, thus demonstrating that the correction for expansion velocities standardizes the luminosities of SNe II significantly. It is important to mention that when the sample is restricted to eight objects with $cz < 3000 \text{ km s}^{-1}$, the scatter drops to 0.20 *mag*. This implies that the standard candle method can calculate distances with a precision of 9%, which is comparable to the 7% yielded by SNe Ia.

Overall, the standard candle method is characterized by a scatter of between 0.39 and 0.20 *mag*. In its present form, the method appears very promising for the determination of cosmological distances. It is remarkable that this precision is better than yielded by EPM (Expanding Photosphere Method which will be analyzed later) which yields precision of $\sim 20\%$ in distance or 0.43 *mag* (Hamuy 2001). And the standard candle technique is far less complicated. It requires only a few spectra and photometry around day 50 of the plateau phase. To solve the extinction in the host galaxy, only a few extra photometric and spectroscopic observations are required.

The standard candle method has been applied to find the Hubble constant, using the SN 1987A (this is used because is the only one from the sample having a precise distance in the Cepheid scale). Assuming a large Magellanic cloud distance of 50 kpc, the authors obtained $H_0 = 54 \pm 13$. This value agrees comfortably with the 63 ± 4 value from Cepheids and SN Ia (Hamuy et al. 1996; Phillips et al. 1999). Despite the success of this study, clearly, more calibrators are required to improve this estimate, especially considering that SN 1987A is not a “typical” SN II–P, and shows a non–typical light curve for its class.

In the worst case scenario, the standard candle method can produce distance moduli with a precision of 0.39 *mag* so that 13 SNe II–P at $z = 0.3$ should allow one to measure the distances of such objects with a precision of 5% and provide a robust check on the results of SNe Ia.

ii *The atmospheres of Type II Supernovae and the Expanding Photosphere Method*

Authors: Ronald G. Eastman, Brian P. Schmidt, and Robert Kirshner (1996)

In this paper, the authors use the Expanding Photosphere Method (EPM), to determine distances to SNe II by comparing the photospheric angular size with the expansion velocity measured from spectral lines. The photospheres of SNe II are low density and are dominated by electron scattering, therefore the photospheric flux is dilute relative to a Planck function. The reliability of EPM distances depends on understanding how the dilution is related to physical properties of the supernova atmosphere. For this method, four filter combinations are used: $\{BV\}$, $\{VI_c\}$, $\{BVI_c\}$ and $\{JHK\}$. The main differences may be expressed in terms of the observable color temperature. The effect of uncertain dust extinction on angular size is shown to be small.

This paper is more focused on theoretical simulations of the expanding ejecta of SN II taking into account the blackbody distribution of the emergent flux. By running sophisticated codes to model individual SNe, the authors obtain a more accurate distance estimate. These atmosphere models and optical distance correction factors require time consuming and computationally demanding procedures, all of which goes beyond the scope of this thesis. However, the final applications are quite interesting; a comparison between the EPM distances obtained and the Cepheid distances obtained to a set of SNe II–P.

The application of the EPM to measure distances to SNe II is a very promising technique for determining the extragalactic distance scale and expansion rate of the universe. The typical SNe II–P is $M_B \sim -17$ to -18 . Unlike other empirically established correlations (some poorly understood) the physical basis of EPM is controllable, because the emitting gas is the simplest possible (H). The EPM can be modeled accurately with current available information. In this study, the particular phase used to model the distances is at the moment of recombination of hydrogen (~ 5000 K), which in red supergiant explosions (RSG), explains the extended plateau observed in SNe II–P. The author’s model for a photospheric phase Type II supernova atmosphere is a hydrogen dominated, optically thick, homogeneous expanding shell, moving at velocities $\sim 10^6$ to 10^7 ms^{-1} .

The EPM works with the plateau phase (from ~ 20 days to 140 days); beyond the plateau phase, the bolometric light curve tracks the instantaneous energy input rate from radioactive decay, the electron scattering optical depth is of order unity, and it is no longer possible to obtain accurate distances with EPM. Table 3.3 summarizes the current EPM distance scale and corresponding available Cepheid distances. The two methods show remarkable consistency:

EPM and Cepheid Distances to Type II-P Supernovae							
SN	Galaxy	V_{pec}^a (km s^{-1})	V_{pec}^b (km s^{-1})	A_v ($m\text{ag}$)	EPM Distance (Mpc)	Cepheid Distance(Mpc)	
1968L	NGC 5236	380	380	0.11	$4.5_{-0.8}^{+0.7}$	4.1 ± 0.4	
1969L	NGC 1058	620	620	0.18	$10.6_{-1.1}^{+1.9}$	9.29 ± 0.69	
1970G [†]	NGC 5457	380	390	0.44	$7.4_{-1.5}^{+1.0}$	7.5 ± 0.8	
1973R	NGC 3627	450	460	2.7	15_{-7}^{+47}	...	
1979C [†]	NGC 4321	1300	1150	0.45	15_{-4}^{+44}	17.1 ± 1.8	
1980K [†]	NGC 6946	320	310	1.2	$5.7_{-0.7}^{+0.7}$...	
1986L	NGC 1559	1110	1110	0	16_{-2}^{+42}	...	
1987A [†]	LMC	0.6	$0.049_{-0.006}^{+0.006}$	0.051 ± 0.003	
1088A	NGC 4579	1300	1150	0	20_{-3}^{+43}	17.1 ± 1.8	
1989L	NGC 7331	1420	1440	1	17_{-4}^{+44}	...	
1990E	NGC 1035	1230	1240	1.7	18_{-2}^{+43}	...	
1990K	NGC 150	1420	1440	0.5	20_{-5}^{+6}	...	
1990ae	anon0020+06	7800	7800	0.5	115_{-25}^{+35}	...	
1992H	NGC 5377	2240	2159	0	31_{-4}^{+44}	...	
1992af	ESO 340-G3	5380	5400	0	55_{-20}^{+25}	...	
1992am	anon0122-04	14500	14500	0.3	180_{-25}^{+35}	...	
1992ba	NGC 2082	950	940	0.3	$14_{-1.5}^{+1.5}$...	

SNe also analyzed by Hamuy and Pinto (2002).

[†] SN also analyzed by Weiler et al. (1998).

Table 3.3:

$$\frac{D_{\text{Cepheids}}}{D_{\text{EPM}}} = 0.98 \pm 0.08 \quad (3.12)$$

This suggests that any systematic differences between the two methods are very small.

The authors recommend that the results of this paper be applied only to SN II–P during the plateau phase. The common SNe II–P having a plateau duration of ~ 80 to 150 days, in which the resulting SN is expected to be spherical to a high degree of accuracy, making SNe II–P excellent candidates for applying EPM. Compared to SN II–P, other SNe types are much less suitable for application of EPM, including SNe such as SNe II–pec, SNe II–n, as well as SNe Ia.

Despite the large number of parameters introduced to specify the model atmospheres, and the corresponding broad range of spectral behaviors they display, the distance correction factors themselves exhibit a behavior which is very nearly one–dimensional. The results of this work indicate that with good B , V , and I photometry, EPM can measure distances to SNe II–P with an accuracy of 5% to 10%. When using only B , V photometry, the uncertainty is approximately twice as large. Infrared photometry is free from the influence of line absorption, which dominates B –band based color temperatures during the

recombination epoch, and it should give results comparable to using optical photometry.

iii *Radio Supernovae as Distance Indicators*

Authors: Kurt W. Weiler, Schuyler D. Van Dyk, Marcos J. Montes, Nino Panagia and Richard A. Sramek (1998)

In this paper, the authors show that the radio light curves of radio emitting supernovae (RSNe) evolve in a systematic fashion with a distinct peak flux density being reached at each frequency, with a well defined time from explosion to peak. For example, at 6cm wavelength the peak spectral luminosity $L_{6\text{ cm peak}}$, and time after explosion date t_0 to reach that peak $t_{6\text{ cm peak}} - t_0$, are found to be related. If this relation (given at the end of this review) is supported by further observations, it provides a way for determining distances to SNe, and thus to their parent galaxies, from purely radio continuum observations. This study was realized with the Very Large Array; with its current sensitivity, it is possible to employ these relations for objects out to ~ 100 Mpc.

In this study, a special effect has been noticed; SNe II appear to have higher 6 cm radio luminosity at peak if they take longer to reach that peak. This effect is consistent with the theory of the SN shock/CSM interaction model of Chevalier (1982a, 1982b, 1984) for the origin of the radio emission if, for the more inhomogeneous SN II, this arises in diverse circumstellar environments; the denser the CSM, the longer it takes for the material to become optically thin to the radio emission and the brighter it will be. If this effect is quantified, it can provide a purely radio based secondary distance indicator for SNe (and their host galaxies).

Although the relations described above are empirical, there is some support based on theory of the following properties:

- (1) Nonthermal synchrotron emission with high brightness temperature.
- (2) A decrease in absorption with time, resulting in a smooth, rapid turn-on first at shorter wavelengths and later at longer wavelengths.
- (3) A power-law decline of the emission flux density with time at each wavelength after maximum flux density (absorption $\tau \approx 1$) is reached at that wavelength.
- (4) A final, asymptotic approach of spectral index α to an optically thin, nonthermal, constant negative value (Weiler et al 1986; Weiler, Panagia, & Sramek 1990).

Chevalier (1982a, 1982b) proposed that the relativistic electrons and enhanced magnetic field necessary for synchrotron radio emission are generated by the outgoing shock wave from the SN explosion which is interacting with the high-density envelope of ionized CSM. This CSM is also the source of the initial absorption. The radio light curve that results from these two competing effects of rapidly declining absorption and more slowly declining

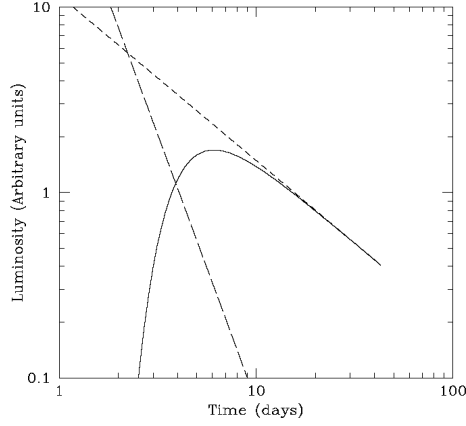


Figure 3.9: Representation of the competing effects of rapidly declining absorption (long-dashed curve), and more slowly declining emission (short-dashed curve), which yield the characteristic rapid turn-on and slower turn-off light curve (solid curve), observed for RSNs at any given frequency (Weiler et al. 1998).

emission is shown schematically for one frequency in Figure 3.9. In Figure 3.10 is shown that the peak luminosity at any frequency is related to the time interval after explosion required for the radio emission to reach that peak.

It has been shown by Weiler et al (1986) that the radio emission from RSNs can be described, for simple cases, by:

$$S[mJy] = K_1 \left(\frac{\nu}{5 \text{ GHz}} \right)^\alpha \left(\frac{t - t_0}{1 \text{ day}} \right)^\beta e^{-\tau} \quad (3.13)$$

where:

$$\tau = K_2 \left(\frac{\nu}{5 \text{ GHz}} \right)^{-2.1} \left(\frac{t - t_0}{1 \text{ day}} \right)^\delta \quad (3.14)$$

with K_1 and K_2 corresponding, formally to the flux density and uniform external absorption, respectively, at 5 GHz (6 cm wavelength) 1 day after explosion t_0 . The term $e^{-\tau}$ represents the attenuation of a medium that completely and uniformly covers the emitting source. The parameter δ describes the time dependence of the optical depth for the uniform external absorbing medium. The emission from the RSN is assumed to be nonthermal synchrotron radiation with spectral index α and to be decreasing with time with index β . It should be noted that in order to fit the SNe II-pec and SNe II-n radio light curves, it would be necessary to add additional absorption and some correction terms to equations: (3.13) and (3.14). Table 3.4 shows the flux density, time from explosion to reading 6 cm peak luminosity, peak 6 cm luminosity and assumed distances and radio distances to the sample SNe.

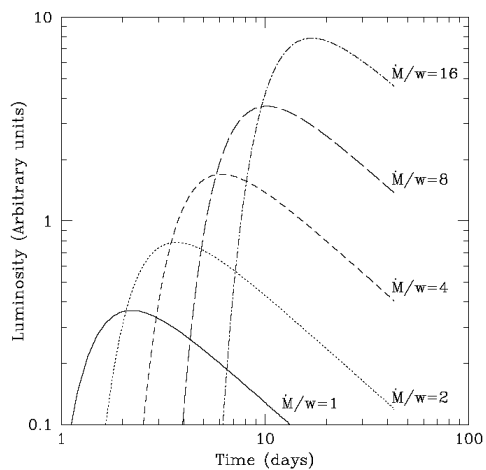


Figure 3.10: Representation of the radio light curves at a given frequency for SNe with differing mass-loss rate per supernova. Note that the longer the time delay required to reach peak luminosity, the higher is that luminosity peak (Weiler et al. 1998).

Radio Supernova Properties and Distances						
SN	Optical Type	P 6cm flux density $S_{6\text{cm peak}}$ (mJy)	Time from explosion ($t_{6\text{cm peak}} - t_0$) (days)	$L_{6\text{cm peak}}$ (10^{28} ergs s^{-1} Hz $^{-1}$)	Assumed Distance (Mpc)	Radio Distance (Mpc)
1970G	II-L	21.25±3.25	307.0±37.5	14.0±3.25	7.4±0.6	7.4±1.05
1978K	II	229.0±47.5	685±19	55.3±20.2	4.5±0.7	3.9±0.8
1979C	II-L	7.3±0.2	605.0±49.3	25.3±5.4	17.1±1.8	20.1±2.15
1980K	II-L	2.5±0.1	140.0±28.5	1.2±0.4	6.3±1.0	12.7±1.95
1981K	II	5.1±2.1	33.8±36.4	2.1±1.2	5.9±1.1	3.3±1.1
1985L	II-L	0.7±0.15	309.0±67.5	3.6±1.3	21.6±3.2	42.5±8.5
1986E	II-L	0.3±0.1	224.0±25.5	1.4±0.45	19.4±2.9	49.0±8.3
1986J	II-n	136.0±4.6	1150.0±53	199.0±60.05	11.1±1.7	7.2±1.1
1987A [†]	II-pec	91.4±70.5	1.0±1.3	0.003±0.0025	0.051±0.002	0.71±0.1
1988Z	II-n	1.9±0.1	1420±95.5	237±71.35	102.6±15.4	70.7±10.65

SNe also analyzed by Eastman, Schmidt, and Kirshner (1996).

[†] SN also analyzed by Hamuy and Pinto 2002.

Table 3.4:

Because of the very diverse nature of the data, missing data at critical (usually early) times, and variations in the assumptions for the modeling of different RSNe, it is extremely difficult to assign errors. The authors presented evidence that the radio emission from SNe may have quantifiable properties that allow for distance determinations. RSNe II, based on the sample of objects, appear to obey a relation: $L_{6\text{ cm peak}} \cong 5.5 \times 10^{23} (t_{6\text{ cm peak}} - t_0)^{1.4}$ ergs $\text{s}^{-1} \text{ Hz}^{-1}$ (with time in days). Thus, measurement of the radio turn-on time ($t_{6\text{ cm peak}} - t_0$) and peak flux density ($S_{6\text{ cm peak}}$) can yield a luminosity estimate and therefore a distance.

After reviewing these three papers, we can reach the following conclusions:

SNe II-P are believed to originate only in intermediate mass stars of 8–12 M_{\odot} , which are in the red supergiant range; higher mass stars produce the other Type II subtypes (Smartt et al. 2001). This finding reduces considerably the initially believed SNe II-P degree of heterogeneity. SNe II-P are typically $M_B \sim -17$ to -18 , with a plateau phase lasting from about ~ 80 to 150 days (Eastman et al 1996). Also, although SNe II are not as bright as SNe Ia, they are the most common type of SN, and even though display a wide range in luminosity at all epochs, SNe II-P offer the potential to be used as distance indicators (Hamuy and Pinto 2002). The expanding shell moves at velocities $\sim 10^6$ to 10^7 ms^{-1} , through which radiation diffuses to the surfaces and then escapes (Eastman et al. 1996). The EPM applied by Eastman, Schmidt and Kirshner, reports an accuracy of 5% to 10% and according to them is a “powerful and precise technique for studying the extragalactic distance scale”. The Standardized candle method applied by Hamuy and Pinto (2002), reports a scatter of about ~ 0.4 to 0.3 mag ($\sim 10\%$ in distance), concluding their method to be “very promising for the determination of cosmological distances”. In the paper of Weiler et al. (1998), the authors estimated errors from the flux density error from table 3.3 but no specific values were given. The future of SNe II-P looks much better than it did a few years ago, thanks to the development of better telescopes, observations and simulation techniques. Despite this, it is remarkable that the authors of the three analyzed papers (and from other references), were not able to give concluding evidence due to the fact that there are not enough observations of SNe II. A definitive answer of SNe II applications, benefits and limits will require the design of an intensive search in those galaxies where the formation of SNe II progenitors seems more abundant. Table 3.5 shows the average adopted absolute bolometric magnitudes $\langle M_{bol} \rangle$ and dispersions $\langle \sigma \rangle$ for SNe Ibc, II-P, II-L and II-n. Note that the values listed for SN II-P represent the dispersion in absolute magnitudes *before* the normalization proposed by Hamuy and Pinto (2002). Table 3.6 summarizes the main average data collected from these three independent studies for the type II-P supernova:

Absolute Magnitudes and dispersion		
SN Type	$\langle M_B \rangle$	σ
SN Ib/c	-18.44	0.39
SN II-P	-17.86	1.39
SN II-L	-18.38	0.51
SN II-n	-20.03	0.6

Adopted maximum absolute B magnitudes and dispersion in the AB-system
 From Miller & Branch (1990), Cappellaro et al. (1997), Cappellaro et al. (1993) and Patat et al. (1994).

Table 3.5:

SNe II-P Average Data					
	Progenitor Star type	Progenitor Mass [Solar Masses]	Bolometric Mag. $\langle M_{bol} \rangle$	Ejecta Velocity (ms^{-1})	Time* to reach peak M_{bol}
Typical $\langle SNe II-P \rangle$	Red Supergiant	~8 to 12 Solar masses	~ -17 to -18	~ 10^6 to 10^7	~10 to 15 (days)
	Time* to reach Plateau Phase	Duration of the Plateau Phase	Precision reached Eastman, Schmidt & K	Precision reached Weiler, Van Dyk etc	Precision reached Hamuy & Pinto
	~20 to 40 (days)	~ 50 to 100 (days)	~5 to 10%	no value reported	~10%

*Times in days after explosion

References:

Hamuy and Pinto (2002).

Eastman, Schmidt, and Kirshner (1996).

Weiler, Van Dyk, Montes, Panagia and Sramek (1996).

Table 3.6:

Chapter 4

DWARF IRREGULAR GALAXIES

4.1 A brief review of the classification of galaxies.

Galaxies are classified by their morphology according to the almost 80 years old Hubble classification scheme which is still used, although with some updates. In this classification system, galaxies are divided in types by their shapes, with the three main types being: Spiral, Elliptical and Irregular. Elliptical galaxies are galaxies essentially of approximately uniform density. Their forms vary among seven ellipticity classes from spherical, $E0$, to highly elliptic $E7$. Obviously, the ellipticity classification depends equally on two factors: the true shape and the angle of orientation under which it is observed. The ellipticity in the En classification is given by: $n = 10(1 - b/a)$ where a is the length of the major axis and b that of the minor. Spiral galaxies are subdivided into two main categories; normal spirals and barred spirals. Normal spirals have a central ellipsoidal nucleus from which emerge spiral shaped arms of stars and interstellar material. The difference with the Barred spiral galaxies is that the spiral arms arise from the ends of a luminous bar of stars and interstellar material. Normal and Barred spiral galaxies are subdivided among three classes: Sa , Sb and Sc according to the degree of openness and tightness of the spiral arms, among other things. More accurately, the subdivision depends on:

- Size of nuclear bulge (Sa = large; Sc = small)
- Openness of spiral pattern (Sa = tightly wound; Sc = open)
- Resolution of arms into supergiant stars and HII regions (Sa = smooth, few small HII regions; Sc = clumpy, lots of bright supergiants & HII regions).

The $S0$ galaxies show some evidence of a central nucleus and the beginnings of a disc and appear to be intermediate between elliptical and spiral galaxies. Figure 4.1 shows the Hubble galaxy classification diagram.

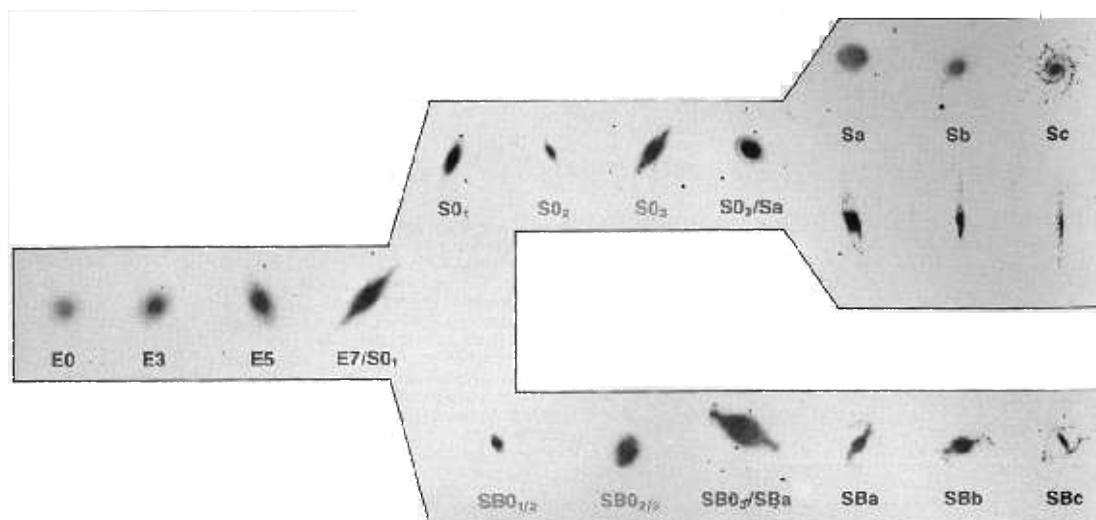


Figure 4.1: The Hubble sequence. From left to right: $E0$ to $E7$ are the elliptical galaxies, $S0$ are intermediate between elliptical and spiral galaxies. Above, normal spiral galaxies and below the barred spiral galaxies (<http://casswww.ucsd.edu/public>).

Irregular galaxies are those galaxies that show neither spiral nor elliptical shape. Major morphological subtypes of these galaxies are formed by the: blue compact galaxies, dwarf irregulars, and giant irregulars (Tosi et al. 2001b). These galaxies are subdivided into two types:

- *Irr-I* having characteristics “beyond” those of class Sc ; high gas content, dominant presence of a young population. *Irr-I* galaxies may show bar-like structures and incipient spiral structure. Such galaxies are sometimes referred to as “Magellanic Irregular” galaxies.
- *Irr-II* which are galaxies which defy classification because of some form of disturbance.

Table 4.1 compares the main galaxy types and their characteristics such as average luminosities, masses, stellar populations, etc.

It should be noted that the observed and classified galaxies are restricted to galaxies large and bright enough to be visible. If a galaxy has too big radius for its magnitude (small surface brightness), then it is not visible. In contrast, if the radius is too small, the galaxy will appear as a star. The dwarf irregular galaxies suffer of the combination of these two factors; faintness and small radius. These are the reasons why these kind of galaxies have long been ignored and little studied.

Galaxy Characteristics Related to Classification						
	E0-E7	S0	Sa	Sb	Sc	Irr
Nuclear Bulge	"All Bulge" No disk	Bulge & Disk	Large	→	Small	None
Spiral Arms	None	None	Tight/Smooth	→	Open/Clumpy	Occasional traces
Gas	Almost none	Almost none	~1%	2-5%	5-10%	10-50%
Young Stars	None	None	Traces	→	Lots	Dominates
HII Regions	All Old (~ 10 ¹⁰ yr)	Old	Some young	→		Appearance Mostly young (but some old)
Spectral Type	G-K	G-K	G-K	F-K	A-F	A-F
Color	Red	Red	→	→	→	Blue
Mass (M _⊙)	10 ⁸ -10 ¹³	(More)	10 ¹² -10 ⁹	(Less)		10 ⁸ -10 ¹¹
Luminosity (L _⊙)	10 ⁶ -10 ¹¹	(More)	10 ¹¹ -10 ⁸	(Less)		10 ⁸ -10 ¹¹

Source : (<http://casswww.ucsd.edu>).

Table 4.1:

4.2 Stellar Populations

Stars are grouped into two general types: Population I and Population II. In the Milky Way galaxy, the criteria for this classification take into account space velocity, chemical composition, age, distribution in the Hertzsprung–Russell, diagram, etc. Studying the composition of a galaxy consists in observations of the strength of spectral absorption lines and broad band colours. The space velocity of a star can be determined by knowing its tangential and radial velocities. All of these measurements allow astronomers to obtain average star masses and chemical composition (metallicity¹). The final result is a population model, giving the stellar composition of the galaxy (Karttunen et al. 1993). After the Big Bang, during the formation of the first generation of stars the only elements available were H and He. The first stars formed and, if massive, they had a relatively short life ($\sim 2 \times 10^7$ to 1.5×10^9 years). Their explosions enriched the universe with heavier elements synthesized in their cores to form the raw but enriched material for subsequent generations of stars called Population I. The low mass stars from the first generation of stars evolved to the present day very slowly. These stars are characterized by a very low metallicity. These stars are

¹In Astronomy, due to the dominant abundance of H ($\sim 90\%$) and He ($\sim 7\%$), the abundance of all elements heavier than H and He is usually referred to as metallicity. Which is defined as follows: $[\text{Fe}/\text{H}] = \log(\text{Fe}/\text{H}) - \log(\text{Fe}/\text{H})_{\odot}$.

Stellar Population Characteristics		
	Population I	Population II
Typical Objects	Supergiant stars Red giants T-Tau stars	Medium and low mass stars Dwarf stars Long Period Variables
Space velocity in the Milky Way	Low	High
Metallicity [Fe/H]	~ 0.02 to 0.04	~ 0.001 to 0.005
Average Age (10^9 years)	~ 1.5 to 0.02	~ 13 to 10
Dust interstellar media	abundant	very little

Data from Karttunen et al. (1993) and Faulkner and De Young (1993).

Table 4.2:

denominated Population II stars. Because of their origin, Population I stars have clouds of dust and gas around and near them, while Population II stars generally are found in interstellar dust and gas free environments. Table 4.2 summarizes the main characteristics of *Pop I* and *Pop II* stars.

According to their intrinsic characteristics, galaxy types have different stellar population ratios. Elliptical galaxies show that practically all their stars were formed simultaneously about 10^{10} years ago and that most of their mass resides in lower main sequence stars of less than one solar mass. The bulges of spirals have a composition similar to that of an elliptical galaxy. This explains the lack of core-collapse supernovae found in Elliptical galaxies and in the bulges of spiral galaxies. On the contrary, arms in typical spiral galaxies are clearly rich in interstellar dust, HII regions and *OB* associations, these latter associations being formed by young stars of spectral type *O* and *B*, so it would be reasonable to expect a large number of SNe II and SNe Ibc to occur there (as we will see detailed in chapter 5). In the case of Irregular galaxies, due to their rich dust and interstellar media, the expected rate of core collapse SNe is also high, but it has to be taken in consideration that these galaxies have on average 0.1 times the mass of a spiral galaxy.

4.3 Where do dwarf irregular galaxies fit in the larger scheme of things?

Dwarf irregular galaxies, considered extreme late-type spirals, and discovered and classified² as a separate class of objects by Haro (1956), are the most numerous type of galaxies thus far discovered in the Universe. They have been considered to be the building blocks of larger massive galaxies and a substantial contributor of mass to the universe. But the difficulties of observing them have not allowed a better understanding of their characteris-

²The whole family was later divided into two subclasses: red and blue, according to their integrated colours (Popescu et al. 1997).

Parameter	Average Properties of <i>dIrr</i>	
	Dwarf Irr	
M_B	-15.5	
Typical $\log(\text{SFR})$	$-2 \pm 1 M_\odot \text{yr}^{-1}$	
Estimated gas mass fraction	0.8	
H-II region diameter	100 pc	
H α luminosity	$1.2 \times 10^{38} \text{ ergs}^{-1}$	

Hunter and Gallagher III (1985).

Table 4.3:

tics. Dwarf irregular galaxies can have masses from 10 to 1000 times smaller than typical spiral and elliptical galaxies and often are of low surface brightness.

A very important issue of dwarf irregular galaxies is that they are extremely rich in interstellar material. The relative amount of gas reaches 15% or more in Irregular galaxies (Karttunen et al. 1993). This, combined with the numerous galaxies of this type in the universe plays a key roll in determining the chemical enrichment of the universe. Furthermore, it is largely believed that due to their abundant interstellar material, certain types of dwarf irregular galaxies are or have been very active in star formation. The resulting young populations of stars, will generate massive stars (*Pop I*) stars, some of which will evolve into red supergiants with masses between³ ~ 8 and $12 M_\odot$, the SNe II Progenitors! A basic property of galaxies is the star formation rate (*SFR*), which will be described and calculated in chapter five. Table 4.3 shows some of the average properties of Dwarf Irregular Galaxies at distances up to 15 Mpc.

Also, dwarf irregular galaxies are playing an increasingly large role in cosmology. This is because if as predicted by modern cosmology, dwarf galaxies were more abundant in the early universe, then it would be reasonable to expect many SNe II at cosmological distances (high red-shifts).

Due to the faintness and compact size of dwarf irregular galaxies, these galaxies are intrinsically difficult objects to measure their distances of. But because their presumably high star formation rate (and consequently an expected high SNe II rate), a trustable SNe II distance indicator method would give rise to an excellent alternative to calculate directly the distances to the SNe II host galaxies.

³More massive stars are also generated, but the more massive a star, fewer of them are formed.

Chapter 5

A SUPERNOVA SEARCH IN THE LOCAL UNIVERSE

5.1 Supernova rates in dwarf irregular galaxies.

The rate of SNe is a key parameter, regulating the chemical evolution of galaxies, the kinematics of the interstellar medium, and production of cosmic rays, in addition to being a fundamental constraint for stellar evolution theories (Cappellaro et al. 1997). The rate of each supernova type (and subtype), depends obviously on the availability of progenitors. Every galaxy type has a specific interstellar medium density, dust content and stellar population composition. According to these parameters it is logical to expect a different supernova rate for each SN and galaxy type.

In order to obtain an average rate of SNe many searches by different groups of astronomers have been carried out. The number of SN discoveries in the last decade almost equalled those of the previous century (Cappellaro et al. 1997). Three important search results have been presented by: van den Bergh, Li & Filippenko (2002; hereafter VLF), by Navasaryan, Petrosian, Turatto, Cappellaro & Boulesteix (2001; hereafter NPTCB) and by Eck, Cowan, & Branch (2002; hereafter ECB). In these three studies the authors concluded that SNe Ia occur in all galaxy types and found with high statistical confidence that SNe Ibc and II are mainly concentrated in late-type¹ galaxies. In table 5.1 a comparison table is presented between the final count results of the three searches of SNe and the corresponding classification of their host galaxy.

The results of this comparison are in concordance with the updated Asiago supernova catalogue (Barbon et al. 1999) where 1447 SNe and their host galaxies are reported in table 5.2.

The rate of SN, in particular SN II is found to peak in the late *Scd–Sd* spirals (Cappel-

¹Late type galaxies are the Spirals *Sbc*, *Sc*, *Scd* and *Sd*, and their barred counterparts.

SNe and host Galaxies Classification								
Study Authors [†]	Galaxy Type	SNe Ia	SNe Ibc	SNe II-n	SNe II-L [‡]	SNe II-P [‡]	SNe II	Total SNe II
VLF		15	0	1	-	-	1	2
NPTCB	E	12	0	0	0	0	0	0
ECB		0	0	0	0	0	0	0
VLF		5	2	0	-	-	8	8
NPTCB	Sa/SBa	2	0	0	1	0	3	4
ECB		0	0	0	1	0	0	1
VLF		8	2	0	-	-	2	2
NPTCB	Sab/SBab	3	0	0	0	0	2	2
ECB		0	0	0	0	0	0	0
VLF		21	2	2	-	-	17	19
NPTCB	Sb/SBb	14	2	1	1	2	7	11
ECB		1	0	0	1	2	0	3
VLF		6	6	1	-	-	12	13
NPTCB	Sbc/SBbc	13	5	3	0	0	13	16
ECB		0	0	1	0	0	0	1
VLF		6	7	4	-	-	18	22
NPTCB	Scd/SBcd	21	13	3	3	5	40	51
ECB		0	1	0	3	6	3	12
VLF		0	0	0	-	-	2	2
NPTCB	Ir	2	1	0	0	0	2	2
ECB		2	1	0	1	0	0	1

[†] From the NPTCB Study, the data used for this table, is the sum of the isolated, pair and group member galaxies.

[‡] Unfortunately the VLF study, does not classify SNe II-P nor SNe II-L ranking them just as SNe II.

Table 5.1:

	I	II	III	IV	V	VI	VII	VIII	IX	X	XI	XII	XIII	XIV	XV	XVI	XVII	XVIII	XIX	XX	Total	
I	10	2	5	9	3	8	6	13		2											18	77
Ia	24	31	6	20	13	28	32	35	10	5		1	18								187	410
Iapec	3	4			2	1	3	2		1			1						1		1	19
Ib			1		1	1	1	9	1										1	1	1	17
Ib/c							2	2		1		1	1								2	9
Ic			1	1	1	2	3	9	2				4								4	27
Iac						2																2
II			2	7	5	32	23	73	12	8	3	1	11	1	2	6					56	242
IIb					1			2	1			1										5
II-n			1	1		5	4	10	1			1			2						9	34
IIpec					1		1	4				1									2	9
Pec				1	1	1		1	1												2	7
nc	38	14	15	32	16	62	42	91	7	8	1	6	58		2	19	1	177			589	
Total	75	51	31	72	43	143	116	251	35	25	4	10	96	1	5	28	2	459			1447	

Notes: nc means not classified supernovae and/or galaxies.

Table 5.2: Distribution of supernovae according to the morphological types of their parent galaxies (Barbon et al. 1999).

Galaxy Type	Mass range	<Average Mass>
<i>Sbcd</i> Galaxies	$10^9 - 10^{12} M_{\odot}$	$\sim 10^{10} M_{\odot}$
<i>Irr</i> Galaxies	$10^8 - 10^{11} M_{\odot}$	$\sim 10^9 M_{\odot}$

Table 5.3:

Study Authors	# of SNe in <i>Irr</i>	# of SNe in <i>Sbc</i>	# of SNe in <i>Scd</i>	# of SNe / M_r
VLF	2	13	22	2/Mr = 20
NPTCB	2	16	51	2/Mr = 20
ECB	1	1	12	1/Mr = 10
Asiago †	10	27	111	10/Mr = 100

† Because many of the Asiago Catalogue SNe were observed before the actual SNe classification, many SNe have not been properly classified.

Table 5.4:

laro et al. 1997). All data available support these conclusions and this has been confirmed by various authors.

The SN number in irregular galaxies appears consistently low, but we have to realize that in order to compare the irregular and the spiral galaxies SN ratio, we need to normalize the SN number by the galaxy masses (Table 5.3):

$$\Rightarrow \text{Mass ratio } M_r = \frac{M(Irr)[M_{\odot}]}{M(S)[M_{\odot}]} = 0.1 \quad (5.1)$$

where $M(Irr)$ represents the typical mass of a *dIrr* galaxy and $M(S)$ that of a typical Spiral.

If we adjust the number of SNe II in Irregular galaxies for the VLF, NPTCB, ECB and the Asiago search, with the mass ratio M_r . We obtain a normalized number of SNe II according to the galaxies mass, compared in table 5.3 with the number of SNe II in *Sbc* and *Scd* galaxies. Instead of normalizing the supernova rate as we do here by galaxy mass (which often is only indirectly known) one encounters more generally the SN rate normalized by luminosity, which is a measured quantity.

Note that the normalized number of SNe II in *Irr* Galaxies is of the order of the number of SNe II in *Scd* Galaxies: $\# \text{ SNe II in } Scd \sim \# \text{ SNe II} / M_r$. This suggests us roughly that we should observe 10 *Irr* galaxies for each *Scd* Galaxy, something that does not seem very difficult since Irregular Galaxies are the most numerous galaxy type in the Universe.

A basic property of all galaxies is the star formation rate (*SFR*) which is the first step to derive the Supernova Rate (*SNR*). One of the most popular methods to derive *SFRs* from optical observations is by measuring the Balmer line fluxes, which are very sensitive to the HII regions surrounding massive young stars (Weilbacher & Alvensleben 2001). The Balmer lines are formed when an H atom recombines into an excited state and subsequently returns to the ground state via a sequence of radiative transitions (Karttunen et al. 1993). Most of these Balmer lines, involve the transition $n = 3 \rightarrow 2$, that will lead to the emission of an H_α photon. The relation between the number of recombinations and ionizations (in completely ionized H which is approximately the case of a HII-region) is: $n_{rec} \propto n_i^2$. In order to calculate the *SFR* of an HII-region, one has first to obtain the H_α Luminosity $L(H_\alpha)$. As an example we will review the $L(H_\alpha)$ of the Blue Compact Dwarf Galaxy HS0016+1449 studied by Popescu et al. (1995), which has a high degree of ionization and thus a considerable expected *SFR*. Taking the $L(H_\alpha) = 4.74 \times 10^{39}$ [ergs $^{-1}$], we can obtain the *SFR* from equation 5.2

$$L(H_\alpha)[\text{ergs}^{-1}] = \nu^2 \cdot SFR[M_\odot\text{yr}^{-1}] \quad (5.2)$$

where the ν^2 -factor is 6.97×10^{41} for the blue compact dwarf galaxy HS0016+1449.

$$SFR[M_\odot\text{yr}^{-1}] = \frac{L(H_\alpha)[\text{ergs}^{-1}]}{\nu^2} [M_\odot\text{yr}^{-1}] = 6.80 \times 10^{-3} [M_\odot\text{yr}^{-1}] \quad (5.3)$$

This *SFR* means that we expect the formation of 0.0068 stars per year in this galaxy. Once we have obtained the *SFR* for the HS0016+1449 BCDG², we will proceed to derive the *SNR* for this galaxy. The reason for choosing this galaxy is simple: it is in this galaxy that the first (and possibly the only up to now) supernova was observed in a Dwarf Irregular Galaxy (Popescu et al. 1995). SN 1995ah is a type II, suggested to belong to the II-L subclass. The calculation of the Supernova Rate (*SNR*), depends on the *SFR* and the initial mass function which is the relation between the number of stars Φ_M , formed with mass m :

$$\Phi_M = \Phi_m^{-2.5} \quad (5.4)$$

where Φ_0 is a constant.

The supernova rate *SNR* is related to the Star formation rate *SFR* as follows:

$$N(\geq 10 M_\odot) = \int_{10}^{100} \Phi_0 m^{-2.5} dm = \Phi_0 \left[-\frac{2}{3} m^{-\frac{3}{2}} \right]_{10}^{100} = 2.04 \times 10^{-2} \Phi_0 \quad (5.5)$$

where $N(\geq 10)$ is the number of stars with mass greater or equal to $10 M_\odot$

²A blue compact dwarf galaxy reinforces the idea of abundant massive star formation due to its high degree of ionization and blue continuum, which reflects the presence of young, massive stars which are the progenitors of SNe II.

$$M(\geq 10 M_{\odot}) = \int_{10}^{100} m \Phi_0 m^{-2.5} dm = \Phi_0 \left[-2m^{-\frac{1}{2}} \right]_{10}^{100} = 4.32 \times 10^{-1} \Phi_0 M_{\odot} \quad (5.6)$$

where $M(\geq 10)$ is the number of stars with mass greater or equal to $10 M_{\odot}$ multiplied by the star mass. This is the amount of mass involved, forming stars with mass $M \geq 10 M_{\odot}$

$$\begin{aligned} \Rightarrow SNR &= SFR \frac{N(\geq 10 M_{\odot})}{M(\geq 10 M_{\odot})} = \frac{\int_{10}^{100} \Phi_0 m^{-2.5} dm}{\int_{10}^{100} m \Phi_0 m^{-2.5} dm} SFR = \frac{2.04 \times 10^{-2} \Phi_0}{4.32 \times 10^{-1} \Phi_0 M_{\odot}} SFR \\ &= 4.72 \times 10^{-2} M_{\odot}^{-1} SFR = (4.72 \times 10^{-2} M_{\odot}^{-1})(6.8 \times 10^{-3} M_{\odot} \text{yr}^{-1}) \end{aligned} \quad (5.7)$$

$$\therefore SNR = 3.21 \times 10^{-4} \text{yr}^{-1}$$

Thus, the supernova rate for the HS0016+1449 blue compact dwarf galaxy is approximately $3.21 \times 10^{-4} \text{yr}^{-1}$. This SNR is in good concordance with the supernova rate for irregular galaxies = $3.26 \times 10^{-4} \text{yr}^{-1}$ obtained by Cappellaro et al. (1997). Although in equations 5.5 and 5.6 the integral limits are from $10 M_{\odot}$ to $100 M_{\odot}$, taking into account stars including those more massive than $17 M_{\odot}$, which won't produce SNe II, but Ibc. Actually, according to the IMF (equation 5.4), the probability of super-massive star production drops with $m^{-2.5}$ so it practically vanishes when m grows.

5.2 Investigation of the feasibility of a targeted search for type II supernovae of predominantly type II–P in dwarf galaxies.

Before deciding to prepare a dedicated SNe II search we need to quantify how feasible such a targeted search in *dIrr* galaxies might be. Taking the supernova rate calculated for the BCDG (discussed above) we get: If the SNR is: $3.21 \times 10^{-4} \text{yr}^{-1} \Rightarrow$ it would take 3.11×10^3 years for a SN II to occur! Or if we want a SN II per year in this kind of galaxies, we would need to observe 3.11×10^3 galaxies of the same type per year. This doesn't look too promising. However, it should be noted that the values used by Popescu et al. (1997) might not be representative. In fact Weillbacher and Fritze v. Alvensleben (2001) report a calibration for the ν^2 factor which is rather $1.41 \times 10^{41} \text{ergs}^{-1}$ instead of $6.90 \times 10^{41} \text{ergs}^{-1}$. Moreover, the SFR for HS0016+1449 appears to be very low. Values more commonly found are in the range $SFR \approx 0.1 M_{\odot} \text{yr}^{-1}$ (Weillbacher & Fritze). Using this SFR value in equation 5.7, we obtain a SNR of:

$$\begin{aligned} \Rightarrow SNR &= 4.72 \times 10^{-2} M_{\odot}^{-1} SFR = (4.72 \times 10^{-2})(1.0 \times 10^{-1} M_{\odot} \text{ yr}^{-1}) \\ \therefore SNR &= 4.72 \times 10^{-3} \text{ yr}^{-1} \end{aligned} \tag{5.8}$$

Although this SNR is about an order of magnitude higher we still need to take into account that this is the SNR for all SNe II types. If we want to restrict the search to SNe II–P these number obviously would be reduced: In the NPTCB search there are a total of 86 SNe II whereas only 7 were classified as SNe II–P. In the ECB search, 18 SNe II were reported of which 9 are SNe II–P (the VLF search nor the Asiago Catalogue give a sub–classification for SNe II). So we should multiply our SNR by a factor of ~ 0.5 to 0.08, a fact that dramatically lowers our expectations for finding a SN II–P.

With all the collected data and information, it can be seen that the design of a specific targeted search for SNe II–P during the plateau–phase in $dIrr$ is a demanding task. This is due to the low finding–probability and hence, elevated number of galaxies (or years) needed to observe.

Despite these facts, this point of view is very conservative (may be too much). Here are some further points to consider before discarding the feasibility of a targeted search for SNe II–P.

- The problem that appears to arise when we restrict the search from SNe II to SNe II–P, is not actually a dramatic restriction. This is because according to the Initial Mass Function (equation 5.4), which governs the number of stars formed of a specific mass, the formation of higher mass stars is inhibited. So, noting that the SN II–P progenitor is the lowest mass of all core–collapse supernovae progenitors, we can expect that approximately ~ 0.5 of all core–collapse SNe would be SNe II–P.
- The low SFR and thus SNR could not be accurate, this is because recent studies (Weilbacher & Fritze v. Alvensleben 2002), showed that the SFR for $dIrr$ galaxies is not constant over time. Instead, it comes in starbursts when the the SFR increases to up to $\sim 5\text{--}20 M_{\odot}$! During this period the SNR would vary proportionally, making a targeted search for SNe II–P feasible.
- This specific search has been restricted for SNe II–P in $dIrr$ galaxies but, it would be reasonable to include in the search late–type spirals due to their predominance in Pop I stars. Fact that would improve the finding rate.
- An important aspect that has to be considered is that any search for SNe II would increase statistics and provide valuable observational data. This will allow further analysis of core–collapse SNe.

Finally it is remarkable that a targeted search for SNe II–P in $dIrr$ galaxies to our knowledge has not yet been proposed, which is suggested in this work.

Chapter 6

CONCLUSIONS

As mentioned in the introduction, one of the greatest problems in Astronomy has been determining reliable distances. Supernovae, as one of the most energetic events in the universe, can be observed out to great distances. The brightest supernovae are SNe Ia; they are the result of the detonation of an accreting white dwarf which has gone beyond the Chandrasekhar limit ($\sim 1.4 M_{\odot}$). As a result SNe Ia are likely to have the same intrinsic luminosity. That is the reason why these objects are widely used as standard candles, and why they are ideal for determining distances.

Another SN type is formed by the core-collapse supernovae. This type of SNe comes from the explosion of a giant star ($\geq 8 M_{\odot}$) which has arrived at its final evolutionary stage. After consuming all its core hydrogen, nuclear fusion stalls and the star is not able to support gravity any longer. The star contracts and T and P increase until the helium produced by the hydrogen fusion (in core-collapse SNe mainly by the CNO cycle) ignites. Eventually the core (now formed by He) gets to high enough temperatures and pressures to initiate the triple- α process. The chain of fusion continues to produce heavier and heavier elements (which after the SN explodes will enrich the universe!) until it reaches ^{56}Fe . At this point, because Iron is the element with the highest binding energy, there is no longer energy being released through fusion. The star now collapses on a dynamical time scale for this process and explodes, ejecting the outer layers at velocities $\sim 10^6$ to 10^7 ms^{-1} . If core-collapse SNe can be used to derive distances like their SNe Ia counterparts, there would be an alternative distance measuring method.

Although core-collapse SNe are not as bright as SNe Ia, they occur especially frequently in late type galaxies (such as *Scd*) and irregular galaxies, objects in which SNe Ia are rare. Dwarf irregular galaxies (*dIrr*) are considered the building blocks of the universe. If these galaxies are actively forming massive *Pop I* stars, it would be reasonable to think that there could be core-collapse events.

One of the aims of this thesis was to find out if it is possible to use core-collapse SNe as a standard candle. To do this, first of all a general review was needed of the

two major progenitor mechanisms of SNe, and the characteristic behavior of their light curves and spectra. Because there are several subtypes of core-collapse SNe, an analysis of each subtype's specific characteristics was made in order to decide which supernova subclass was the most likely candidate whose intrinsic luminosity can be calibrated. Type II-P supernovae, thanks to their special properties appear to have a smaller degree of heterogeneity and magnitude spread. Especially in the plateau phase (having a duration between ~ 50 to 100 days), the luminosity remains approximately constant, allowing a better normalization and thus, a more accurate distance calculation.

The second aim of this thesis was to make an investigation on how feasible and desirable it would be to design a specific, targeted search for SNe II-P. The abundance of dwarf irregular galaxies is well known, as is their predominance in Population I stars. Calculations of the star formation rate of a blue compact dwarf galaxy (a *dIrr* galaxy presently actively forming stars), gave the following results; a rather low supernova rate ($\sim 3.21 \times 10^{-4} \text{ yr}^{-1}$ to $4.72 \times 10^{-3} \text{ yr}^{-1}$). This low rate, could be thought to be an optimistic rate, because in our goal to find SNe II-P to derive distances, first we have to restrict the *SNR* according to the ratio: SNe II-P / SNe II. However this ratio should not be an excessive restriction, as seen in Chapter 5 we concluded to expect an approximately ~ 0.5 ratio, which in fact is encouraging because it implies the predominance of SNe II-P over other SNe II subtypes.

It is remarkable that there is no current accurate information about SN rates in *dIrr*. An interesting possibility is suggested by the recent studies published by Weilbacher and Fritze v. Alvensleben (2002) where the authors confirm strong evidence of a non-constant star formation rate, with starbursts occurring during the life of a *dIrr*. This star formation by starbursts enhances the feasibility of a targeted search for SNe II-P in *dIrr*. If the galaxies targeted for the search are restricted to galaxies during a starburst, when the *SFR* increases to up to $\sim 5\text{--}20 M_{\odot}$, then the expected *SNR* for these galaxies would vary proportionally, making the search feasible. Furthermore, in a final design of a targeted search of SNe II-P, besides *dIrr* galaxies, it would be a good idea to include in the search the late-type spirals due to their predominance of Population I stars. This with the purpose of increasing the SN detection rate.

Lastly, we have to consider that SNe Ia have been largely studied and used as distance indicators. Specific targeted searches for SNe Ia have been successfully developed and carried out. So to make the use of SNe II-P as distance indicators possible, the first step is obviously to have a large data base in order to characterize statistically their properties and improve the distance indicator methods. Then, any search for SNe II-P would increase statistics and therefore contribute to a better understanding of these events. A targeted search for SNe II-P in *dIrr* galaxies to our knowledge has not yet been proposed, a search such as that proposed in this work which would lead to plenty of material for further investigation and analysis.

Chapter 7

Appendix

7.1 Appendix A: Hydrostatic Equilibrium

The hydrostatic equilibrium is the relation between two tremendous forces which govern the structure of a star: the force of gravity and the thermal pressure. Gravity tends to constrict all stellar material towards its centre. This tendency is counteracted by the pressure generated by the thermonuclear reactions through the thermal motion of the gas. To be stable a star must be in mechanical equilibrium, and must not expand or contract significantly.

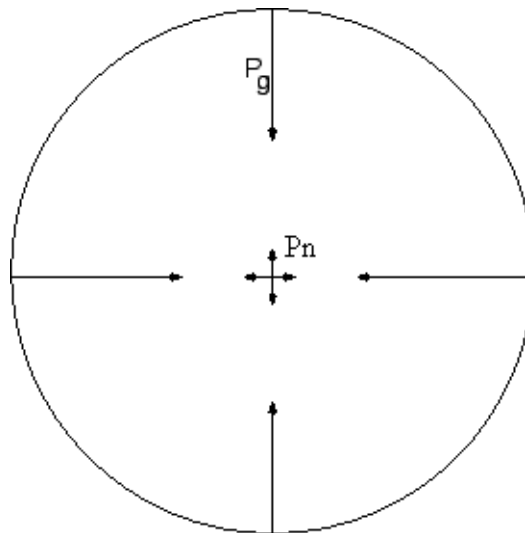


Figure 7.1: Hydrostatic Equilibrium is reached in a star when the resultant between gravitational and nuclear pressure is zero (<http://tesla.phys.unm.edu/>).

In order to have Hydrostatic Equilibrium in a star, the sum of the inward pressure and the outward pressure must be zero. We will call P_n the Nuclear Pressure and P_g the gravitational Pressure.

$$\begin{aligned} P_n + P_g &= 0 \\ \Rightarrow P_n &= -P_g \end{aligned} \tag{7.1}$$

If we consider a star of *uniform density and temperature*¹, then we can obtain the gravitational pressure from the gravitational force.

$$P = \frac{F}{A} \tag{7.2}$$

We can consider the star as being formed by thin shells. Each one contributing with a dP_g pressure:

$$dP_g = -\frac{Fg}{S} \tag{7.3}$$

where:

$$\begin{aligned} S &= 4\pi r^2 \\ Fg &= G \frac{m_{shell} M_{Total}}{r^2} \\ \Rightarrow dP_g &= -G \frac{m_s M_T}{4\pi r^4} \end{aligned}$$

where:

$$\begin{aligned} \rho &= \frac{m}{V} \Rightarrow m = \rho V \\ m_s &= \rho S = 4\rho\pi r^2 dr \\ M_T &= \int_0^r m_s dr = \frac{4}{3}\rho\pi r^3 dr \end{aligned}$$

Substituting M_T and m_s we get:

$$dP_g = -G \frac{(4\rho\pi r^2)(\frac{4}{3}\rho\pi r^3)}{4\pi r^4} dr \tag{7.4}$$

To calculate the net gravitational pressure we sum the pressure from all shells:

¹Of course, this consideration is not very realistic, but it permits us to make a rough first approximation of the hydrostatic equilibrium condition.

$$\begin{aligned}
\Rightarrow P_g &= - \int_0^R G \frac{(4\rho\pi r^2)(\frac{4}{3}\rho\pi r^3)}{4\pi r^4} dr \\
&= -\frac{4}{3}G\rho^2\pi \int_0^R r dr = -\frac{2}{3}G\rho^2\pi R^2
\end{aligned} \tag{7.5}$$

where:

$$\rho = \frac{M_T}{\frac{4}{3}\pi R^3}$$

$$\therefore P_g = -\frac{3}{8}G \frac{M_T^2}{\pi R^4}$$

Now, the expression for the nuclear pressure P_n . If we assume a pure Hydrogen star (again, not very realistic), from the ideal gas law we know:

$$PV = nk_B T \tag{7.6}$$

where n is the number of particles in the star, T the temperature and k_B is the Boltzman constant (m_H is the Hydrogen mass).

$$P_n \sim \frac{nk_B T}{V_T}$$

where:

$$n = \frac{M_T}{m_H}$$

$$V_T = \frac{4}{3}\pi R^3$$

$$\Rightarrow P_n \sim \frac{M_T k_B T}{\frac{3}{4}\pi R^3 m_H}$$

So we make equal P_n and $-P_g$:

$$P_n = -P_g$$

$$\frac{M_T k_B T}{\frac{3}{4}\pi R^3 m_H} = \frac{3}{8}G \frac{M_T^2}{\pi R^4}$$

(7.7)

$$\frac{k_B T}{m_H} = G \frac{M_T}{2R}$$

$$\therefore M_T = \frac{2k_B T R}{G m_h}$$

This is the total mass M_T a star must have in order to maintain Hydrostatic Equilibrium. We have to notice that the total mass M_T is a function of the Radius R of the star and the star Temperature (which is also a function of R).

By the time the burning H is exhausted (leaving a He nucleus), a drastical drop in P_n occurs which disturbs the Hydrostatic Equilibrium of the star. The violent increase in the core density raises the temperature as the core decreases in size. Once a temperature $\sim 10^8$ K is reached, the He begins to burn and the nuclear reactions follow as will be described in Appendix B until the star nuclear fuel is exhausted.

When the nuclear fuel is exhausted, the pressure (P_n) supporting the gravity (P_g) suddenly stops. The star begins to collapse and to degenerate, this is known as the dynamical time scale for collapse. Which is the time it takes since the Hydrostatic Equilibrium is broken and the star begins to collapse as a Supernova.

7.2 Appendix B: Nuclear reactions in high-mass stars (SN progenitors)

The stellar energy source is the nucleus; there the high pressures and temperatures are large enough for thermonuclear fusion reactions to take place. In these reactions, light elements will be transformed into heavier ones. The resulting nucleus mass is smaller than the sum of the masses of the initial nuclei of the reaction. This difference of mass is called the binding energy, and will be released according to Einstein's relation $E = mc^2$. The nuclear binding energy per nucleon (Q) is given by:

$$Q = \frac{1}{A} [Zm_p + Nm_n - m(Z, N)] c^2 \quad (7.8)$$

Legend:

m_p	Proton mass
m_n	Neutron mass
Z	Atomic number
N	Neutron number
$m(Z, N)$	Mass of the nucleus
$A = Z + N$	Atomic weight

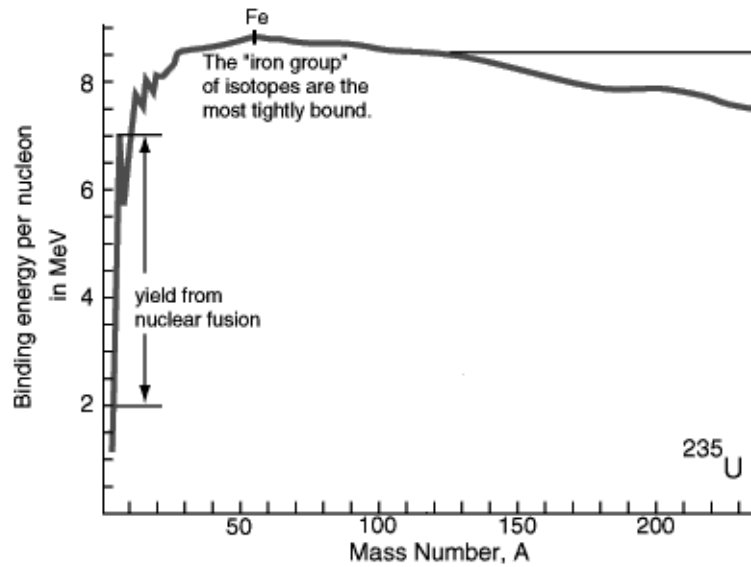


Figure 7.2: Nuclear binding energy per nucleon curve as function of the mass number (A). Notice that ${}^{56}\text{Fe}$ has the maximum binding energy of all elements, reason why it is the heaviest element which can be synthesized by nuclear fusion (<http://hyperphysics.phyastr.gsu.edu>).

The initial composition of a star has a hydrogen abundance of 0.7, helium of 0.28, and metals (any element heavier than ${}^4\text{He}$) of 0.02. The He to H abundance ratio is set by the condition of thermonuclear fusion during the Big-Bang. There are two “hydrogen to helium” consumption processes which compete with each other: the proton–proton (pp) chain and the Carbon–Nitrogen–Oxygen (CNO) cycle. Rate and dominance of the cycles depends on two factors:

- i) There must be C, N and O present for the CNO cycle to occur, however, only a very small amount is required and this condition is often fulfilled.
- ii) The reactions have different temperature dependences.

We can observe how the pp Chain dominates at lower temperatures, but with rising temperatures there is a sudden transition to the CNO cycle, which has an energy production rate that varies strongly with temperature. This is the reason the CNO cycle is more important at higher temperatures and thus for larger mass stars like Supernova progenitors: the red supergiant stars. Here we present a brief overview of the p-p chain and the CNO cycle.

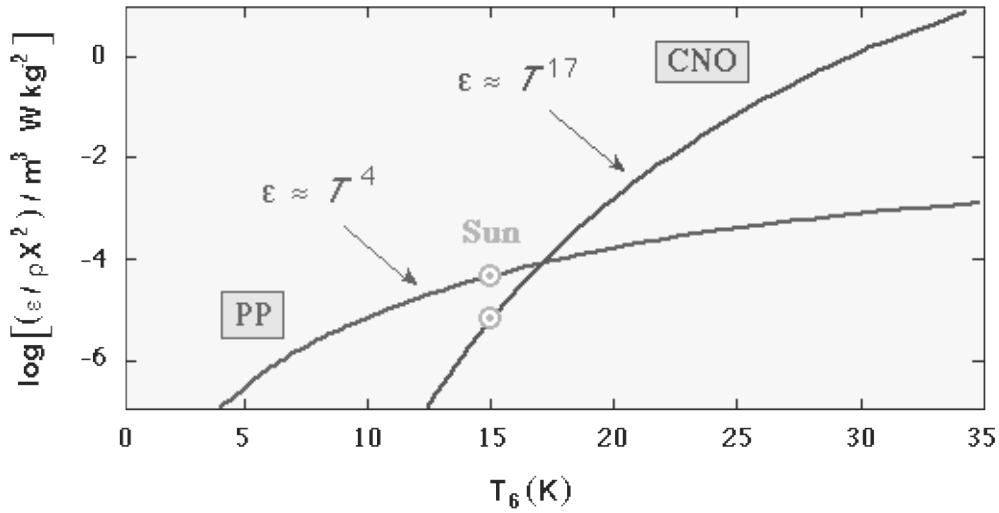


Figure 7.3: Energy production rates for the pp chain and CNO cycle as a function of temperature [units of 10^6 K](<http://csep10.phys.etk.edu>).

The pp Chain

This chain is the dominant sequence of reaction for stars with masses about that of the Sun or smaller. The p-p chain converts Hydrogen to Helium in three main stages.

- (1) ${}^1p + {}^1p \rightarrow {}^2H + e^+ + \nu_e$
- (2) ${}^2H + {}^1p \rightarrow {}^3He + \gamma$
- (3) ${}^3He + {}^3He \rightarrow {}^4He + {}^2H$ [*ppI branch*]

We have to notice that the reaction (1) where a proton collides with another one to form a deuteron² (2H), is a reaction with a very small probability. This reaction (1), requires an average expected time of $\sim 10^{10}$ years! On the other hand, the reaction (2) has an expected time of ~ 1 sec, and reaction (3) an expected time of $\sim 10^6$ years. So reaction (1) is the one that controls the rate of the nuclear “burning”, and permits low mass stars (thus lower core temperature stars $\leq 1.5 \times 10^7$ K) like our Sun to have greater lifetimes.

After reaction (1) is done, the positron (e^+) liberated is immediately annihilated together with an electron (e^-), producing two γ -photons. The neutrinos (ν_e), elementary particles with no electric charge, very weak interaction with other matter (only via the weak interaction) and mass close to but not equal to zero, escape directly from the stellar

²Here we mention that because of the high temperatures all atoms are stripped from their electrons: ${}^2H \rightarrow {}^2H^+$

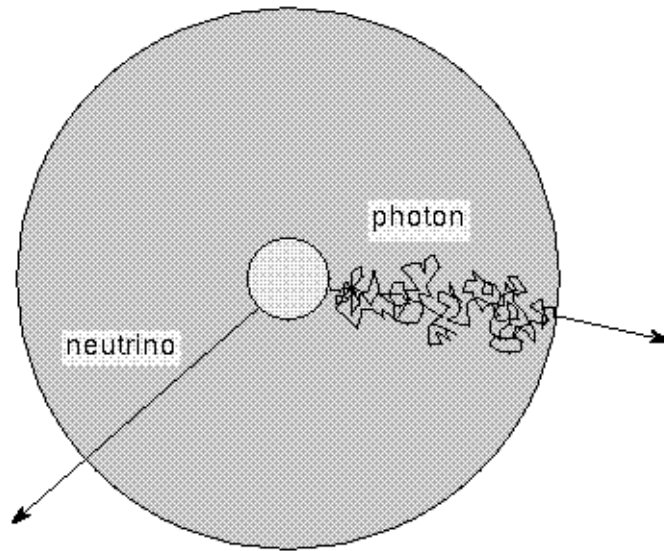
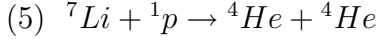
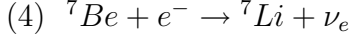
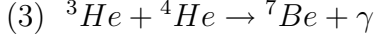


Figure 7.4: Comparison between the paths that a photon and a neutrino must follow. A neutrino will escape without any interaction from the star, while the γ -photon suffers multiple absorption and re-emission processes. This processes, will require about 10^7 years to get from the star's core to outer space, with a wavelength shift from γ -ray to the optical regime (<http://www.mira.org/museum/photon.html>).

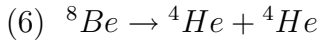
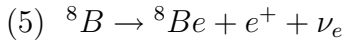
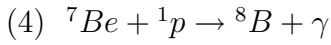
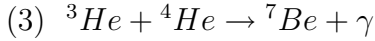
interior after being generated in reaction (1). This free escape across the star, contrasts with the extreme random and “difficult” path that a γ -photon follows since its creation, until radiated into space. The intervening scattering, absorption and re-emission process will take an average travel time from the star core to outer space of about 10^7 years! And will shift the γ -photon into a lower energy photon (in main sequence stars to the visible wavelength range).

Reaction (2) combines the product of the first one (Deuterium, 2H) and a proton to produce 3He (an isotope of Helium) and a γ -photon. For each reaction (3), reactions (1) and (2) have to take place twice, in order to produce the 3He pair needed and to generate the final product: a Helium nucleus (4He) plus 2 protons. However, reaction (3) is not the only possible final reaction. After (1) and (2) are completed, two different sets of reactions can occur, and we will call them the *ppII* and *ppIII* branches. The *ppII* branch is responsible for less than 10% of the energy production, while the *ppIII* branch is responsible for less than 0.1%. Here we have the *ppII* and *ppIII* sequences:

ppII branch:

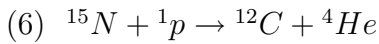
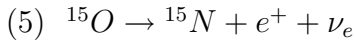
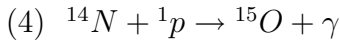
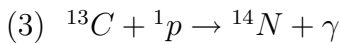
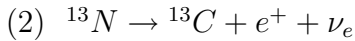
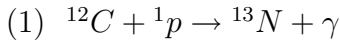


ppIII branch:



The CNO Cycle

For stars with masses below $1.5 M_\odot$ and 2×10^7 K (core temperature), the pp chain is the main source of energy. However, for stars above this mass, the core temperature goes high enough to enable the CNO cycle as the dominant energy production mechanism, despite the fact that the pp chain is still working. This is because for the CNO cycle the reaction rate increases more rapidly with temperature. This process uses Carbon (C), Nitrogen (N) and Oxygen (O) as catalysts for the production of Helium (He). The CNO cycle is obviously the dominant energy source for type II SNe progenitor stars.



In reaction (2), ${}^{13}\text{N}$ is unstable and beta decays to the ${}^{13}\text{C}$ isotope, which has a half-life of ~ 10 min. also generating a positron which will be annihilated and a neutrino which escapes. The ${}^{15}\text{O}$ in reaction (5), undergoes beta decay just like reaction (2) but producing ${}^{15}\text{N}$ instead. We notice that reaction (4) is the slowest of the cycle, and thus determines

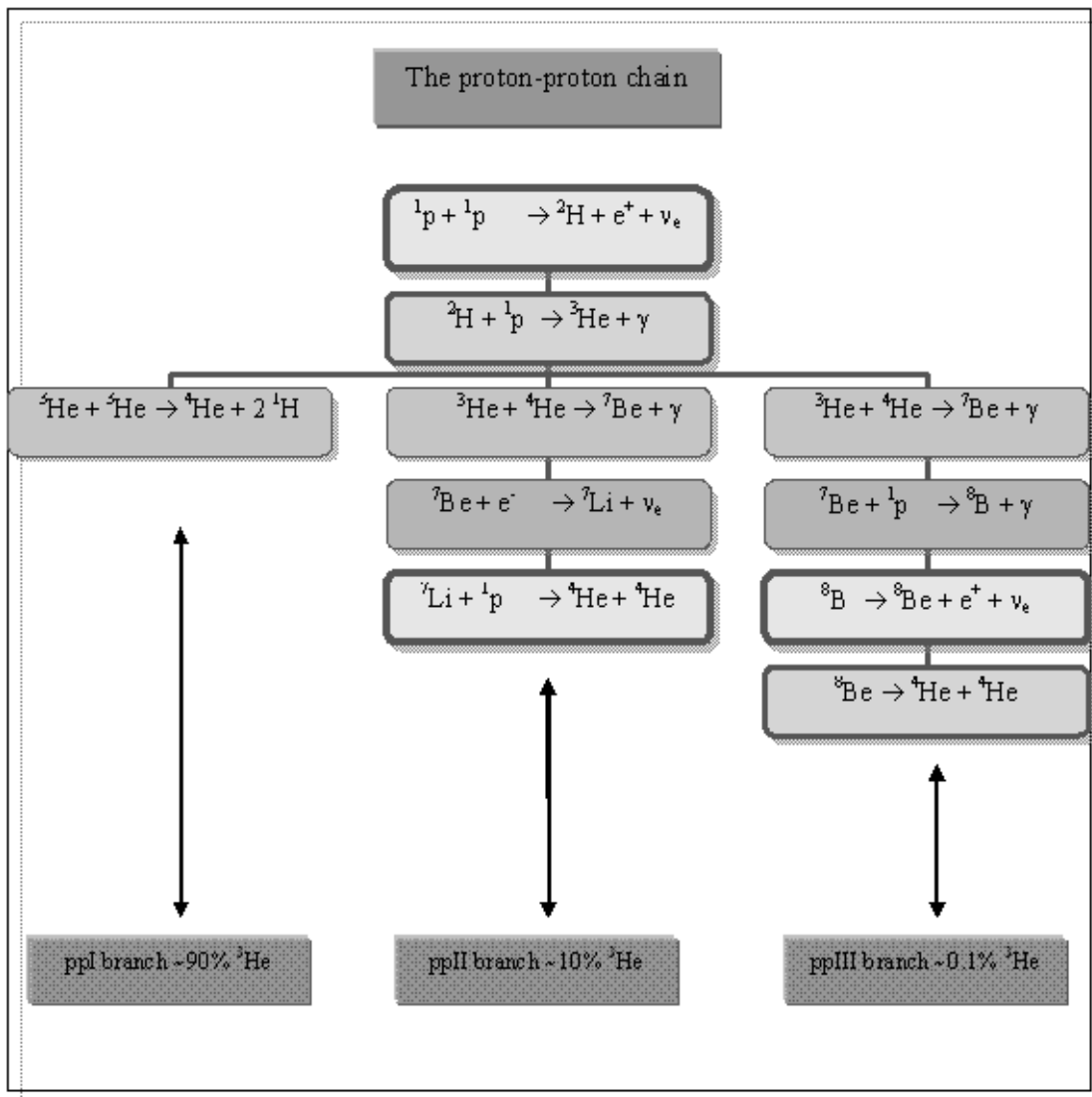


Table 7.1: The proton-proton chain. In the *ppI branch*, four protons are transformed into one Helium nucleus, two positrons, two neutrinos and radiation. Below the branches are the rates of each set of reactions. The pp-cycle is the most important energy source in stars with mass below $1.5 M_{\odot}$ (Karttunen 1993).

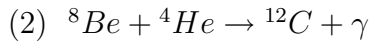
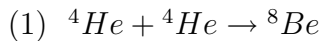
the CNO cycle ratio. At a temperature of 2×10^7 K this reaction has an expected time of 1×10^6 years. Although this is a large time, it is relatively short compared to the 1×10^{10} years expected for the first reaction of the pp chain. This is in complete concordance with the speed of burning and the total life time of stars of different mass.

Notice that along the way various positrons, neutrinos and gamma-rays are produced as the decay products from the unstable isotopes. These are a source of energy in addition to the pp chain gamma-rays. Finally it is remarkable how the number of CNO atoms does not change during the cycle; they serve as catalysts, only converting 4 protons into one ${}^4\text{He}$ nucleus.

The Triple- α Process

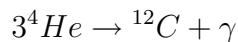
Either via the pp chain or the CNO cycle, the net result of H burning is Helium, which eventually will fill the star's core. The He produced cannot undergo fusion reactions at the current core temperature. As a result of the H decrease, the fusion rate goes down, and the energy production ratio drops. Obviously nuclear pressure drops as well, and because of hydrostatic equilibrium, the star suffers a slight contraction which will heat up the core again until its temperature goes above 10^8 K.

At those temperatures, a highly improbable reaction begins; the fusion of two ${}^4\text{He}$ to form ${}^8\text{Be}$, which added to another ${}^4\text{He}$ will get ${}^{12}\text{C}$ and a γ -photon.



Beryllium 8 is unstable and tends to decay immediately before it can undergo any further reactions. This fact is known as the “Mass 5 and Mass 8 Bottlenecks” which comes from a basic fact of nuclear physics: there are no stable isotopes of any element having atomic masses (A) 5 or 8. So although it would be reasonable to expect that ${}^4\text{He}$ would fuse with a ${}^1\text{p}$ to form a mass 5-isotope or two ${}^4\text{He}$ to form a mass 8-isotope (${}^8\text{Be}$), these products are so unstable that they would fly apart before further reactions. But when core temperatures reach 10^8 K, ${}^8\text{Be}$ is produced at a fast enough rate that there is always a very small equilibrium concentration of ${}^8\text{Be}$ at any one instant during burning reactions (<http://csep10.phys.utk.edu>).

This amount of ${}^8\text{Be}$ can undergo reactions with a ${}^4\text{He}$ to produce an excited (*) ${}^{12}\text{C}$ which emits a γ -photon to become a stable ${}^{12}\text{C}$, this is the triple- α process. The reaction is often written:



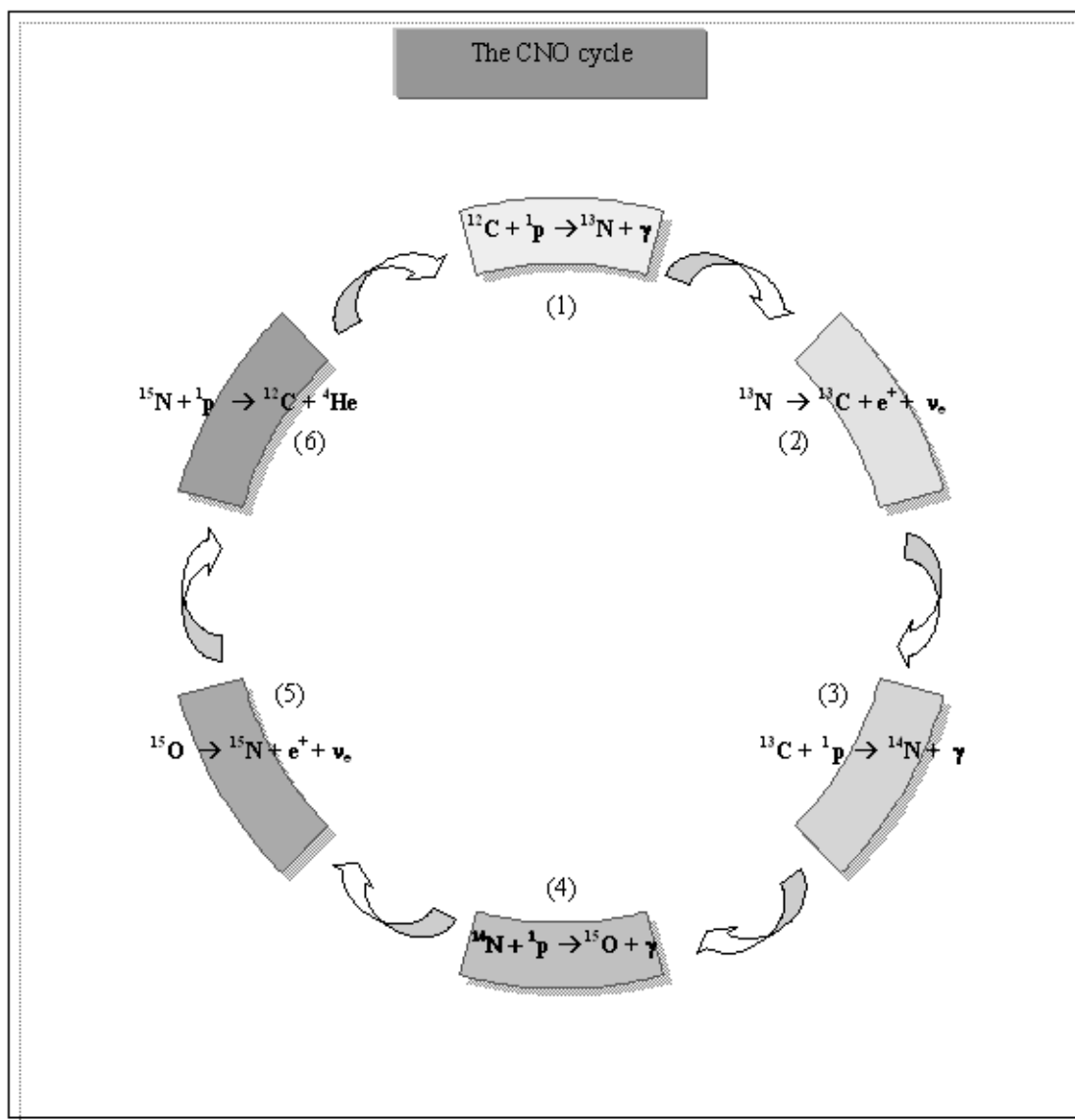


Table 7.2: The CNO cycle is catalyzed by ^{12}C . It transforms four protons into a helium nucleus, two positrons, two neutrinos and radiation. It is the dominant energy source for stars more massive than $1.5 M_{\odot}$. The number of CNO atoms remains constant, acting only as catalysts (based on <http://zebu.uoregon.edu>).

After the core Helium is exhausted, the process of:

- i Lowering fusion rate and cooling.
- ii Loss of nuclear pressure.
- iii Star contraction.
- iv Rise of Core temperature.
- v Onset of new nuclear reactions (burning now the result of the triple- α process, forming Carbon).

is repeated again and again producing heavier elements as the result of the previous burning stage. However, such advanced burning in stars becomes each time a more complicated processes. Each stage up requires higher and higher temperatures in order to overcome greater Coulomb barriers. As the masses increase, the energy production efficiency goes down.

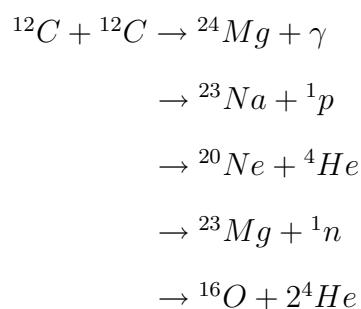
Alpha Reactions

The formation of Oxygen takes place during the Helium burning phase, because of the reaction of some Carbon nuclei with Helium.



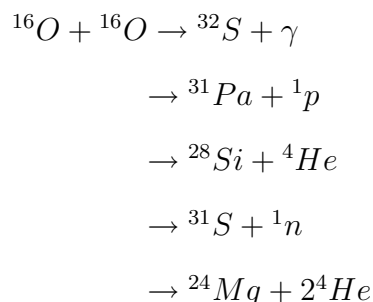
Carbon Burning

Once core Helium is consumed and a temperature ~ 5 to 8×10^8 K is reached, the following reactions can take place:

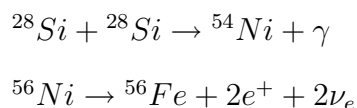


Oxygen Burning

At higher temperatures, Oxygen starts to fuse in similar reactions to the Carbon burning ones:



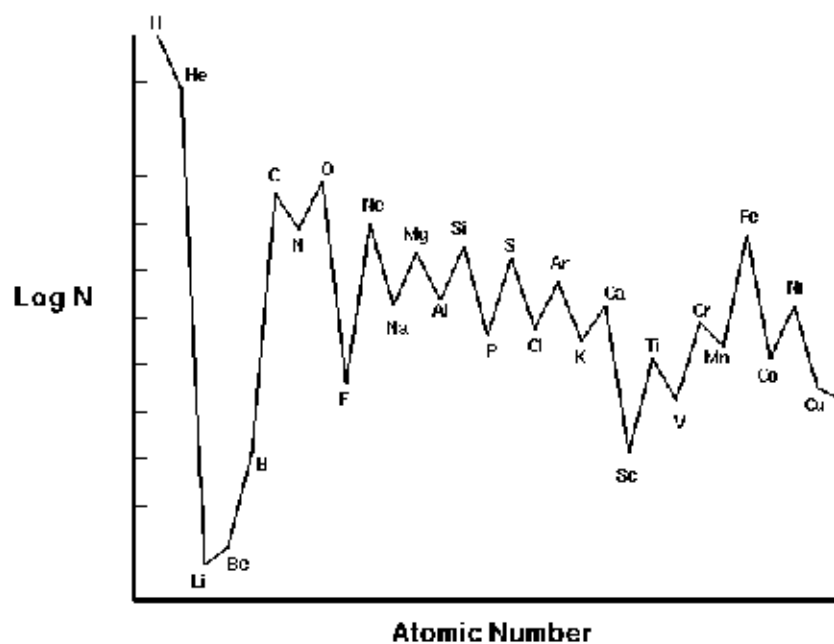
The process keeps fusing elements at higher temperatures producing heavier nuclei and liberating less energy. After several steps, the Silicon begins to form Nickel and Iron.



At this point, because Iron is the element with the highest binding energy, there is no longer fusion taking place to form heavier elements. Any nuclear reaction which involves Fe will breakup the Fe nucleus instead of forming a heavier one, not liberating energy but consuming it. When the temperature goes over 10^9 K, a sequence that involves the disintegration of nuclei by high energy photons in the plasma becomes possible in a process called photonuclear reactions or photodissociations. The formation of heavier nuclei than ${}^{56}\text{Fe}$ is performed through the successive capture of neutrons, with beta decays, and build up to nuclei as far as ${}^{209}\text{Bi}$. Heavier elements than ${}^{209}\text{Bi}$ will only be produced in the violent explosion of SNe. This is the model for the production of the elements of the periodic table, this process is in concordance with the approximate abundance of elements in the universe.

Approximate Abundance of Elements in the Universe					
Element	Abundance (%)	Element	Abundance (%)	Element	Abundance (%)
H	87	Al	0.0002	Cu	-
He	12	Si	0.003	Zn	-
Li	-	P	0.00003	Se	-
B	-	S	0.002	Br	-
C	0.03	Cl	-	Sr	-
N	0.008	K	0.000007	Mo	-
O	0.06	Ca	0.0001	Ag	-
F	-	Cr	-	Sn	-
Ne	0.02	Mn	-	I	-
Na	0.0001	Fe	0.002	Pt	-
Mg	0.0003	Ni	-	Au, Hg,	-
				Pb	-

Table 7.3:

Figure 7.5: Relative element abundance plot: $\ln N$ as a function of the atomic number.

Bibliography

- [1] Barbon R, Buondi V, Cappellaro E, and Turatto *The Asiago Supernova Catalogue – 10 Years After, 1999* Astronomy & Astrophysics. 139:531–536
- [2] Benítez N, Riess A, Nugent P, Dickinson M, Chornock R, Filippenko A. *The Magnification fo SN 1997ff, The Farthest Known Supernova*, 2002 The Astrophysical Journal. 577:L1–L4
- [3] Bressan A, Della Valle M, Marziani P. *On Core–Collapse Supernovae in Normal and in Seyfert Galaxies* 2002 Mon. Not. R. Astron. Soc. 331: L25–L29
- [4] Cappellaro E, Turatto M, Tsvetkov DY, Bartunov OS, Pollas C, Evans R, Hamuy M. *The Rate of Supernovae from the Combined Sample of Five Searches*, 1997 Annu. Rev. Astron. Astrophys. 322:431–441
- [5] Dahlen T, Fransson C. *Rates and Redshift Distributions of High- z Supernovae*, 1999 Annu. Rev. Astron. Astrophys. 350:349–367
- [6] Eastman RE, Schmidt BP, Kirshner R. *The Atmospheres of Type II Supernovae and the Expanding Photosphere Method*, 1996 The Astrophysical Journal. 466:911–937
- [7] Eck CR, Cowan JJ, Branch D. *A Search For Radio Emission From Supernovae With Ages From About 1 Week to More Than 80 Years*, 2002 The Astrophysical Journal. 573:306–323
- [8] Filipenko AV. *Optical spectra of Supernovae* 1997 Annu. Rev. Astron. Astrophys. 35:309–55
- [9] Hamuy M, Pinto P. *Type II supernovae as standardized Candles*, 2002 The Astrophysical Journal. 566:L63–L65
- [10] Hunter D, and Gallagher J. *Star–Forming Properties and Histories of Dwarf Irregular Galaxies: Down But not Out*, 1985 The Astrophysical Journal Supplement Series. 58:533–560

- [11] Karttunen H, Kröger P, Oja H, Poutanen M, Donner K.J. *Fundamental Astronomy*. 2nd Edition. Springer Verlag 1993.
- [12] Leibundgut B. *Cosmological Implications from observations of Type Ia Supernovae*, 2001 *Annu. Rev. Astron. Astrophys.*39:67–98
- [13] Navasardyan H, Petrosian AR, Turatto M, Cappellaro E, Boulesteix J. *Supernovae in isolated Galaxies, in Pairs and in Groups of Galaxies* 2001 *Mon. Not. R. Astron. Soc.* 328:1181–1192
- [14] Pooley D, Lewin WHG, Fox DW, Miller JM, Lacey CK, Van Dyke SK, et al. *X-Ray, and Radio Observations of the Type II Supernovae 1999em and 1998S*, 2002 *The Astrophysical Journal*. 572:932–943
- [15] Popescu C, Rafanelli P, Benetti S, Hopp U, Birkle K. and Elsässer H. *SN 1995ah—the First Supernova Observed in a Blue Compact Dwarf Galaxy*, 1997 *Astronomy and Astrophysics*. 74:52–58
- [16] Scurmann SR, Arnett WD, Falk S.W. *Type II Supernovae: Nonstandard Candles as Extragalactic Distance Indicators*, 1979 *The Astrophysical Journal*. 230:11–25
- [17] Searle L, Sargent L, and Bagnuolo W. *The History of Star Formation and the Colors of Late-Type Galaxies*, 1973 *The Astrophysical Journal*. 179:427–438
- [18] Smartt SJ, Gilmore GF, Tout CA, Hodgkin ST. *The Nature of the Progenitor of the Type II–P Supernova 1999em*, 2002 *The Astrophysical Journal*. 565:1089–1100
- [19] Smartt SJ. *Detecting the Progenitors of core-collapse supernovae*. 2001 *The Astrophysical Journal*. 565:1089–1100
- [20] van den Bergh S. *Classifications of the Host Galaxies of Supernovae*, 2002 *The Astronomical Society of the Pacific*. 114:820–825
- [21] Weillbacher P. and Fritze von Alvensleben U. *On Star Formation Rates in Dwarf Galaxies*, 2001 *Astronomy and Astrophysics* 140:476–481
- [22] Weiler K, van Dyk S, Montes M, Panagia N, and Sramek R. *Radio Supernovae as Distance Indicators*, 1998 *The Astrophysical Journal*. 500:51–58